Efficient Endocytic Uptake and Maturation in *Drosophila* Oocytes Requires Dynamitin/p50

Guojun Liu,* Paulomi Sanghavi,* Kathryn E. Bollinger,† Libby Perry,* Brendan Marshall,* Penny Roon,* Tsubasa Tanaka,‡ Akira Nakamura,‡ and Graydon B. Gonsalvez*,[1]

*Cellular Biology and Anatomy and †James and Jean Culver Vision Discovery Institute, Georgia Regents University, Augusta, Georgia 30912, and ‡Department of Germline Development, Division of Organogenesis, Institute of Molecular Embryology and Genetics, Kumamoto University, 2-2-1 Honjo, Kumamoto 860-0811, Japan

ABSTRACT Dynactin is a multi-subunit complex that functions as a regulator of the Dynein motor. A central component of this complex is Dynamitin/p50 (Dmn). Dmn is required for endosome motility in mammalian cell lines. However, the extent to which Dmn participates in the sorting of cargo via the endosomal system is unknown. In this study, we examined the endocytic role of Dmn using the *Drosophila melanogaster* oocyte as a model. Yolk proteins are internalized into the oocyte via clathrin-mediated endocytosis, trafficked through the endocytic pathway, and stored in condensed yolk granules. Oocytes that were depleted of Dmn contained fewer yolk granules than controls. In addition, these oocytes accumulated numerous endocytic intermediate structures. Particularly prominent were enlarged endosomes that were relatively devoid of Yolk proteins. Ultrastructural and genetic analyses indicate that the endocytic intermediates are produced downstream of Rab5. Similar phenotypes were observed upon depleting Dynein heavy chain (Dhc) or Lis1. Dhc is the motor subunit of the Dynein complex and Lis1 is a regulator of Dynein activity. We therefore propose that Dmn performs its function in endocytosis via the Dynein motor. Consistent with a role for Dynein in endocytosis, the motor colocalized with the endocytic machinery at the oocyte cortex in an endocytosis-dependent manner. Our results suggest a model whereby endocytic activity recruits Dynein to the oocyte cortex. The motor along with its regulators, Dynactin and Lis1, functions to ensure efficient endocytic uptake and maturation.

KEYWORDS microtubule motors; endocytosis; cell polarity; kinesin; dynactin

MICROTUBULE motors such as cytoplasmic Dynein (hereafter referred to as Dynein) and proteins of the Kinesin superfamily play essential roles in cargo transport. Dynein is a minus-end motor and is responsible for the majority of minus-end transport within the cell (Kardon and Vale 2009). Mammalian genomes encode >40 different Kinesins, and most of these move cargo toward the plus-end of microtubules (Hirokawa *et al.* 2009). One type of cargo that is known to be transported by microtubule motors are vesicles of the endolysosomal system.

Cargoes that enter the cell via endocytosis follow numerous sorting pathways that ultimately determine their fate. For example, nutrient receptors such as the Transferrin receptor, are recycled back to the plasma membrane (Mayor *et al.* 1993; Huotari and Helenius 2011). Growth factor receptors and signaling molecules are often targeted for degradation (Beguinot *et al.* 1984; Huotari and Helenius 2011). This is necessary to attenuate growth-promoting signals. Persistent and uncontrolled growth-promoting signals are associated with cancer (Normanno *et al.* 2006). Cargoes that are destined for degradation transit through vesicles that undergo maturation from early endosome to late endosome. Late endosomes eventually fuse with acidic, degradative organelles known as lysosomes. Endocytic maturation involves the progressive and ordered association of specific factors with sorting vesicles (Huotari and Helenius 2011). Consequently, early endosomes are associated with a distinct set of proteins in comparison to late endosomes and lysosomes. However, endocytic maturation represents a continuum. Thus, vesicles of mixed identity can also be observed (Rink *et al.* 2005; Vonderheit and Helenius 2005).

doi: 10.1534/genetics.115.180018
Manuscript received June 29, 2015; accepted for publication August 6, 2015; published Early Online August 10, 2015.
Supporting information is available online at www.genetics.org/lookup/suppl/doi:10.1534/genetics.115.180018/-/DC1.
[1]Corresponding author: Cellular Biology and Anatomy, Georgia Regents University, Augusta, GA. E-mail: ggonsalvez@gru.edu

Studies in mammalian cell lines have demonstrated a role for Dynein in motility of early and late endosomes (Valetti *et al.* 1999; Jordens *et al.* 2001; Driskell *et al.* 2007; Flores-Rodriguez *et al.* 2011). Sorting of epidermal growth factor receptor (EGFR) from internalized Transferrin also appears to require Dynein (Driskell *et al.* 2007). However, whether Dynein is actually required for endosome maturation is unknown. Some studies have hinted at such a role. For example, depletion of Dynein light intermediate chains resulted in enlarged late endosomes (Tan *et al.* 2011). The rate at which EGFR was degraded was also reduced in these cells (Tan *et al.* 2011). In a separate study in which early endosomes were artificially enlarged, Dynein was shown to be required for tubule formation after fusion of early endosomes (Skjeldal *et al.* 2012). The implication of this finding is that Dynein might be involved in sorting cargo within early endosomes during their maturation into late endosomes (Skjeldal *et al.* 2012).

In this study, we used the *Drosophila* oocyte as a model to examine the role of Dynein in endocytic maturation. The *Drosophila* egg chamber contains 16 germline cells surrounded by a layer of somatic cells known as follicle cells. One of the 16 germline cells differentiates to become the oocyte, and the remaining 15 become nurse cells (Spradling 1994). During vitellogenic stages of egg chamber maturation (stages 8–10), there is a tremendous up-regulation of clathrin-mediated endocytosis within the oocyte. During these stages, Yolk proteins bind to the vitellogenin receptor, Yolkless (Yl). After endocytosis, Yl is recycled back to the plasma membrane, whereas Yolk proteins are trafficked through the endocytic pathway and stored in condensed yolk granules (DiMario and Mahowald 1987; Tsuruhara *et al.* 1990; Schonbaum *et al.* 2000). Yolk granules are the functional equivalent of dormant lysosomes and represent the endproduct of Yolk protein endocytosis. The granules serve as a food source for the developing embryo. Thus, a defect in endocytic maturation will be reflected by a loss or reduction in the number of condensed yolk granules, a scenario that has been demonstrated using *rab5* nulls (Compagnon *et al.* 2009).

The Dynactin complex is a core regulator of the Dynein motor. Dynamitin (Dmn/p50) is a central component of this complex. Its overexpression is thought to dissociate the Dynactin complex (Echeverri *et al.* 1996; Eckley *et al.* 1999). Indeed, numerous studies addressing the role of Dynein use Dmn overexpression as a means of inhibiting Dynein activity (Burkhardt *et al.* 1997; Duncan and Warrior 2002; Januschke *et al.* 2002). More recently, Dmn depletion has also been shown to inhibit Dynein activity (Raaijmakers *et al.* 2013). We therefore chose to address the role of Dynein in endocytosis by specifically depleting Dmn in vitellogenic egg chambers. Our results indicate a critical role for Dmn in endocytic uptake of Yolk proteins and in maturation of endocytosed vesicles into condensed yolk granules.

Materials and Methods

Drosophila strains and genetics

Unless otherwise indicated, all fly strains were grown at 25°. Oregon-R was used as the wild-type strain. Additional fly strains used were the following: GFP-Dmn expressed using a maternal tubulin driver (Januschke *et al.* 2002); *dmn* short hairpin RNA (shRNA)-A (generated, 5′-TCAGAAGATTACGGAACTATA-3′); *dmn* shRNA-B (generated, 5′-CCGGACGTGTACGAAACTC CA-3′); *lis1* shRNA (generated, 5′-TAGCGTAGATCAAACAGT AAA-3′); *dhc* shRNA-A (Bloomington Stock Center; #36583, donor TRiP); *eb1* shRNA (Bloomington Stock Center; #36680, donor TRiP); *shi* shRNA (Bloomington Stock Center; #36921, donor TRiP); *rab5* shRNA (Bloomington Stock Center; #51847, donor TRiP); *rab7* shRNA (generated, 5′-AACGATATACCCTACTACGAA-3′), *yl* shRNA (Bloomington Stock Center; #56922, donor TRiP), UASp-*rab5Q88L* (Bloomington Stock Center; #9773, donor Hugo J. Bellen); *rab7T22N* (Bloomington Stock Center; #9778, donor Hugo J. Bellen); pUASp-TagRFPt-2xFYVE (generated); pUASp-GFP-Clc (Jha *et al.* 2012); w[*]; P{w[+mC]=matalpha-GAL4-VP16}V2H (Bloomington Stock Center; #7062, donor Andrea Brand); osk^{84} (Kim-Ha *et al.* 1991); osk^{def} (*Df(3R)p-XT103*; Bloomington Stock Center; no. 1962, donor Thom Kaufman); and GFP-Dmn^{ref} expressed using the germline *vasa* promoter (Sano *et al.* 2002).

The shRNA constructs were cloned as oligos into the *Nhe*I/*Eco*RI site of the Valium22 vector (Ni *et al.* 2011). The constructs were injected and balanced at either Genetic Services or BestGene. The shRNA targeting EB1 was used as a control. The shRNAs were driven by crossing to the abovementioned maternal α-tubulin driver (Bloomington Stock Center #7062). The progeny were fattened on yeast paste for 3 days prior to dissection. An additional maternal α-tubulin driver is available from the Bloomington Stock Center (#7063). It should be noted, however, that this driver is active in early-stage egg chambers in addition to mid- and late-stage egg chambers.

The GFP-Dmn^{ref} construct was generated by cloning into the P[w^1 P-vas-gfp] plasmid (Sano *et al.* 2002). The shRNA-refractory Dmn construct was generated by gene synthesis at Genewiz. The pUASp-TagRFPt-2xFYVE plasmid was generated by cloning the cDNA for TagRFPt (Shaner *et al.* 2008) and the 2xFYVE sequence into the pUASp-attB-K10 vector (Koch *et al.* 2009). The cDNA for TAGRFPt was amplified from Addgene plasmid 42635 deposited by Silvia Corvera (Navaroli *et al.* 2012). The 2xFYVE sequence was generated by gene synthesis at Genewiz. Detailed sequence is available upon request. All three constructs were injected at BestGene.

Immunofluorescence: Immunofluorescence was performed as described previously (Sanghavi *et al.* 2012) with a few modifications. Females fattened on yeast paste were dissected in Schneider's media containing 15% fetal bovine serum (Life Technologies). The oocytes were fixed for 20 min in PBS containing 4% formaldehyde (Pierce; catalog #28908). After fixation, the ovaries were washed in PBST (PBS containing 0.1% triton X-100), blocked, and incubated with antibody. For imaging of microtubules (α-tubulin experiment), ovaries were fixed in 1× PBS containing 8% formaldehyde. This fixation step was performed for 15 min.

In situ hybridization: *In situ* hybridization was performed as described previously (Sanghavi *et al.* 2013).

Antibodies: Unless specifically stated, the indicated dilutions are for immunofluorescence (IF). The following antibodies were used: mouse anti-Dynein heavy chain (Dhc) (Developmental Studies Hybridoma Bank; 1:100; donor J. Scholey); rabbit anti-Khc (Cytoskeleton; 1:150); rabbit anti-GFP (Life Technologies; 1:200); rat anti-GFP (Nacalai USA; 1:700); mouse ant-GFP (Clontech; 1:2000 for Western); mouse anti-LaminDmO (Developmental Studies Hybridoma Bank; clone ADL84.12; 1:100; donor P. A. Fisher); rabbit anti-Staufen (D. St. Johnston; 1:3000); rabbit anti-Glued (V. Gelfand; 1:300) mouse anti-γ-tubulin (Sigma; 1:100 for IF, 1:1000 for Western); mouse anti-clathrin heavy chain (BD Biosciences; 1:150); guinea pig anti-Rab5 (1:3000); rabbit anti-Rab7 (1:800) (Tanaka and Nakamura 2008); mouse anti-BicD (Developmental Studies Hybridoma Bank; 1:100; donor R. Steward); FITC-conjugated mouse anti-α-tubulin (Sigma Aldrich; 1:200); goat anti-rabbit Alexa 594 and 488 (Life Technologies; 1:400 and 1:200, respectively); goat anti-mouse Alexa 594 and 488 (Life Technologies; 1:400 and 1:200, respectively); goat anti-rat Alexa 488 (Life Technologies; 1:200); goat anti-guinea pig Alexa 594 (Life Technologies; 1:400); goat anti-mouse HRP (Jackson Immunoresearch; 1:5000 for Westerns) and goat anti-rabbit HRP (Jackson Immunoresearch; 1:5000 for Westerns). The antibody against Yolkless was generated by injecting rabbits with a mix of the following peptides (Peptide 1-CELEKGHHNQSQIQPWSTSSRS; Peptide 2-QAEHQVHPSEQRIRVESPK). Conjugation of the peptides to an immunogen, injection of the peptides into rabbits, and purification of antibodies specific to these two peptides was performed by Pacific Immunology (Ramona, CA). F-actin was visualized using either FITC- or TRITC-conjugated Phalloidin (Sigma Aldrich).

Endocytic assays and staining

The FM4-64 assay was performed by dissecting ovaries from well-fed females. The ovaries were dissected in Schneider's media containing 15% fetal bovine serum (Life Technologies). FM4-64 (Life Technologies) was added to the sample to a final concentration of 10 μM. The ovaries were incubated with the dye for 30 min, followed by two washes in Schneider's media for 15 min each. The live tissues were mounted onto slides and imaged within 30 min.

The mRFP-RAP reporter was obtained from the lab of Linton Traub (Jha *et al.* 2012). *Escherichia coli* expressing GFT-tagged mRFP-RAP were grown and induced with 0.5 mM isopropyl β-D-1-thiogalactopyranoside (Fisher). The induction of the fusion protein was carried out at room temperate for 6 hr. The bacteria were then harvested by centrifugation and lysates were prepared using the B-PER II reagent (Pierce). To purify the fusion protein, the lysates were incubated with glutathione beads (Pierce) for 2 hr at 4°. The beads were then collected and washed several times with PBST (PBS with 0.1% triton X-100) to remove nonspecifically bound proteins. The fusion protein was eluted off the beads using 10 mM reduced glutathione, dialyzed into PBS, and concentrated using an Amicon Ultra filtration kit (EMD Millipore).

To monitor uptake of mRFP-RAP, ovaries from two to three well-fed females were dissected as described above. The ovarioles were teased apart, and 0.5 μg of mRFP-RAP in a total of 30 μl of Schneider's media containing 15% fetal bovine serum and 0.2 mg/ml insulin (Sigma Aldrich) was then added to the dissected ovaries. The samples were incubated with gentle shaking for either 30 or 120 min. The mRFP-RAP was then removed, and the ovaries were washed twice with Schneider's media. The samples were fixed in PBS containing 4% formaldehyde, DAPI stained to visualize nuclei, and mounted onto slides.

The Lysotracker reagent was obtained from Life Technologies. Ovaries were dissected as described above. The ovarioles were incubated with 100 nM Lysotracker in Schneider's media containing 15% fetal bovine serum and 0.2 mg/ml insulin. The egg chambers were incubated with Lysotracker for 45 min. Next, the dye solution was removed and egg chambers were washed with two changes of PBS. The egg chambers were then fixed in 4% formaldehyde, mounted onto slides, and imaged within an hour.

The Nile red staining protocol was performed as described (Yu *et al.* 2011). In brief, dissected ovarioles were fixed and permeabilized by incubating with PBST for 30 min. The PBST was then removed, and egg chambers were washed with PBS. The egg chambers were then incubated with PBS containing 1% BSA and 20 μg/ml Nile Red (Life Technologies). After 20 min, the staining solution was removed, and egg chambers were washed twice with PBS. The egg chambers were then mounted onto slides and imaged. For imaging, the 488-nm laser was used for excitation, and signal for Nile Red was collected in the 550- to 630-nm range.

Transmission electron microscopy

Dissected ovaries were fixed in 4% paraformaldehyde and 2% glutaraldehyde in 0.1 M sodium cacodylate (NaCac) buffer (pH 7.4). The dissected ovarioles were then embedded within agarose. Stage 10 egg chambers where identified and isolated out of the agarose. The samples were postfixed in 2% osmium tetroxide in NaCac, stained with 2% uranyl acetate, dehydrated with a graded ethanol series, and embedded in Epon-Araldite resin. Thin sections were cut using a diamond knife on a Leica EM UC6 ultramicrotome (Leica Microsystems, Bannockburn, IL), collected on copper grids, and stained with uranyl acetate and lead citrate. Egg chambers were observed in a JEM 1230 transmission electron microscope (JEOL USA, Peabody, MA) at 110 kV and imaged with an UltraScan 4000 CCD camera and First Light Digital Camera Controller (Gatan, Pleasanton, CA).

Microscopy

Samples were imaged on either a Zeiss 510 upright confocal microscope or a Zeiss 780 upright confocal microscope. All

imaging experiments were performed at the Georgia Regents University Cell Imaging Core Laboratory.

Data availability

Strains and antibodies generated for this work available upon request.

Results

Stage-specific depletion of Dmn

Vitellogenesis takes place between stages 8 and 10 of egg chamber maturation. However, Dmn is required for oocyte specification (Januschke *et al.* 2002). As such, loss-of-function mutants in *dmn* never specify an oocyte, and egg chamber maturation arrests at early stages (Januschke *et al.* 2002). Therefore, to address the role of the *dmn* gene in Yolk protein endocytosis, we chose an shRNA-mediated depletion strategy (Ni *et al.* 2011).

Two shRNAs were designed against different regions of *dmn*. The shRNAs were expressed using a maternal α-tubulin Gal4 driver that is primarily active from stage 5 onward (Sanghavi *et al.* 2013). As shown in Figure 1, both shRNAs were capable of depleting Dmn in stage 10 egg chambers (Figure 1, B, D, and F). In contrast, the level of Dmn was unaffected in stage 5 egg chambers expressing *dmn* shRNA-B and only modestly reduced in stage 5 egg chambers expressing *dmn* shRNA-A (Figure 1, A, C, and E). Western blotting analysis of ovarian lysates indicated that expression of *dmn* shRNA-A reduced the level of GFP-Dmn by >10-fold (Figure 1, G and H). Expression of *dmn* shRNA-B resulted in a 4-fold reduction in the level of GFP-Dmn (Figure 1, G and H). Based on these results, we conclude that this strategy is able to effectively reduce Dmn levels during vitellogenic stages.

Depletion of Dmn in mammalian cells results in codepletion of p150/Glued (Raaijmakers *et al.* 2013), another component of the Dynactin complex. We observed a similar result in *Drosophila* oocytes (Figure 1, I, J, and K). One interpretation of this result is that depleting Dmn destabilizes the Dynactin complex. Thus, phenotypes that are observed upon Dmn depletion might correlate more broadly to loss of Dynactin activity.

Dmn depletion phenotypes

To analyze the role of Dmn in endocytosis, we examined yolk content in control and Dmn depleted oocytes. Yolk content is often measured by examining autofluorescence emitted by yolk granules. For these experiments, we displayed autofluorescence using a color-coded range indicator where black pixels indicate no signal, red pixels indicate moderate signal, and white pixels indicate high levels of signal.

As expected, control oocytes displayed robust yolk autofluorescence (Figure 2A). By contrast, reduced autofluorescence was observed in egg chambers depleted of Dmn. Two distinct phenotypes were observed in egg chambers expressing *dmn* shRNA-A. In ~12% of oocytes, yolk autofluorescence was almost completely absent (Figure 2, B and H). When these oocytes were visualized using differential interference contrast (DIC) optics, a few vesicular structures were observed toward the posterior of the oocyte (Figure 2B′). The rest of the oocyte displayed a smooth appearance (Figure 2B′). In the remainder of oocytes expressing *dmn* shRNA-A (88%), yolk autofluorescence could be detected, but at a reduced level in comparison to the control (Figure 2C). Under DIC optics, these oocytes displayed large structures that have the appearance of vesicles (Figure 2C′, arrows, and Figure 2H). Of these two phenotypes, only the latter was observed in egg chambers expressing the weaker shRNA, *dmn* shRNA-B (Figure 2, D, D′, and H). The large vesicles were not limited to stage 10 oocytes. They were also observed in mature stage 14 egg chambers expressing either *dmn* shRNA (Figure 2, E, F, and G). Thus, depletion of Dmn resulted in egg chambers with reduced yolk autofluorescence and large vesicles.

To more precisely define the role of Dmn in endocytosis, we examined uptake of the lipophilic dye FM4-64 using dissected egg chambers. As noted in previous publications, control oocytes displayed robust FM4-64 uptake with the majority of signal concentrated at the posterior pole (Figure 2I) (Vanzo *et al.* 2007; Sanghavi *et al.* 2012). By contrast, egg chambers expressing *dmn* shRNA-A displayed reduced FM4-64 uptake (Figure 2J). Often, these egg chambers contained large vesicles that were positive for FM4-64 signal (Figure 2K, arrows; 49%, $n = 52$). Similar, but milder, phenotypes were observed in egg chambers expressing *dmn* shRNA-B (Figure 2L).

FM4-64 is nonselectively internalized into dissected tissues. By contrast, Yolk proteins are internalized by binding the Yl receptor and subsequently undergoing clathrin-mediated endocytosis (DiMario and Mahowald 1987; Tsuruhara *et al.* 1990; Schonbaum *et al.* 2000). Recently, Jha *et al.* developed an endocytic assay using mRFP-RAP, a pseudoligand for the Yl receptor (Jha *et al.* 2012). In contrast to FM4-64, mRFP-RAP is internalized in a manner that more closely mimics the endocytosis of endogenous Yolk proteins. We therefore analyzed uptake of mRFP-RAP (see *Materials and Methods* for details). After 30 min of uptake in control egg chambers, endocytosed mRFP-RAP was detected at high levels around the oocyte cortex (Figure 2M). By contrast, a reduced amount of mRFP-RAP was endocytosed within the same time frame by Dmn-depleted egg chambers (Figure 2N). To monitor endocytic maturation, we examined mRFP-RAP localization after 120 min of uptake. At this time point, the bulk of mRFP-RAP was observed within the interior of control oocytes (Figure 2O). However, mRFP-RAP was mostly observed at the cortex in Dmn depleted egg chambers, accumulating in large vesicles (Figure 2P, arrow).

We next examined the localization of core endocytic factors. Consistent with published results, Clathrin heavy chain (Chc), Rab5, and Rab7 localized along the cortex in control oocytes (Figure 2Q; data not shown) (Tanaka and Nakamura 2008; Vazquez-Pianzola *et al.* 2014). In egg chambers expressing *dmn* shRNA-A, two phenotypes were observed. In the small percentage of oocytes that were severely compromised (those containing minimal yolk autofluorescence), the endocytic

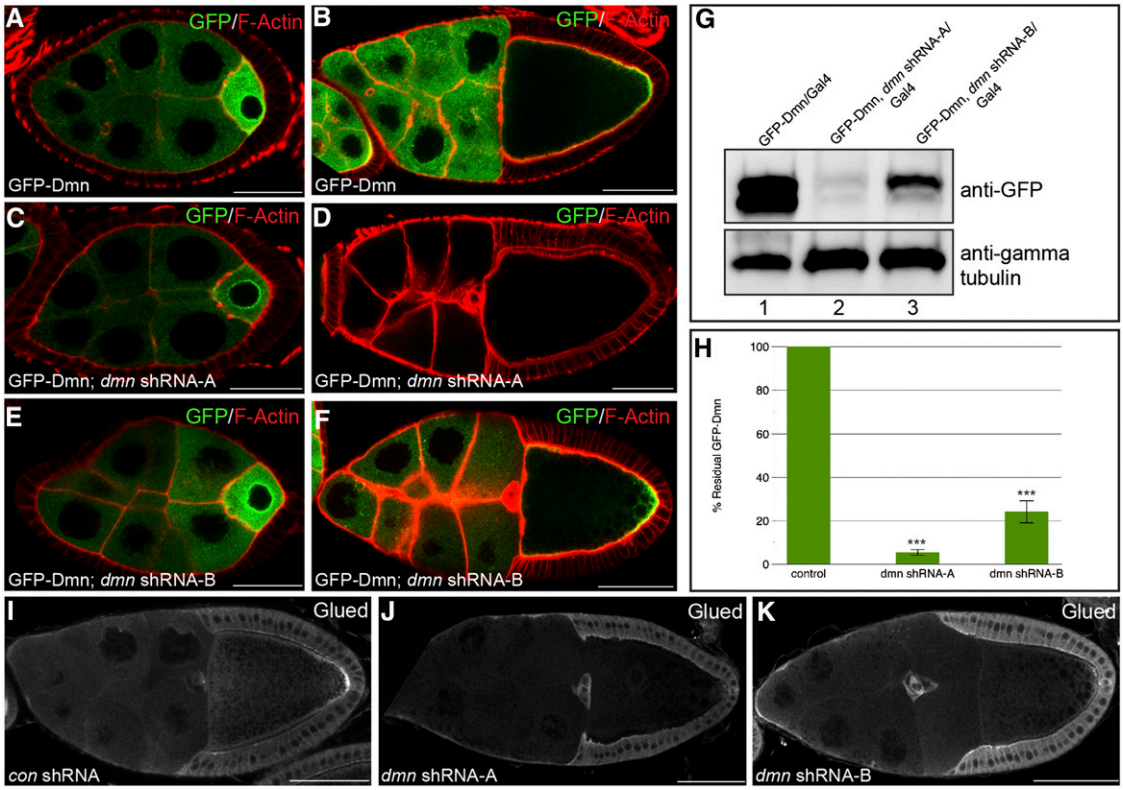

Figure 1 shRNA-mediated depletion of Dmn. (A and B) Egg chambers expressing GFP-Dmn under the control of a maternal tubulin promoter were fixed and processed for immunofluorescence using an antibody against GFP (green). The egg chambers were also counterstained for F-actin (red). Representative stage 5 (A) and stage 10 (B) egg chambers are shown. (C and D) Egg chambers coexpressing *dmn* shRNA-A and GFP-Dmn were fixed and processed for immunofluorescence using an antibody against GFP. Representative stage 5 (C) and stage 10 (D) egg chambers are shown. (E and F) Egg chambers coexpressing *dmn* shRNA-B and GFP-Dmn were fixed and processed for immunofluorescence using an antibody against GFP. Representative stage 5 (E) and stage 10 (F) egg chambers are shown. *dmn* shRNA-A and *dmn* shRNA-B were expressed using a maternal α-tubulin-Gal4 driver (see *Materials and Methods* for details). GFP-Dmn was expressed using a construct in which the maternal tubulin promoter was cloned upstream of the GFP-*dmn*-coding sequence (Januschke *et al.* 2002). (G) Ovarian lysates were prepared from strains expressing GFP-Dmn (lane 1), from strains coexpressing *dmn* shRNA-A and GFP-Dmn (lane 2), or from *dmn* shRNA-B and GFP-Dmn (lane 3). The lysates were run on an SDS-PAGE gel and analyzed by Western blotting using an antibody against GFP (top). The same blot was then probed using an antibody against γ-tubulin (bottom). The level of γ-tubulin serves as a loading control. The images were captured digitally using a UVP bioimaging system. (H) Western blots from three separate experiments depicted in G were quantified using the VisionWorks software (UVP). The level of GFP-Dmn in strains coexpressing *dmn* shRNA-A or *dmn* shRNA-B were compared to the level of GFP-Dmn in the control strain. The error bars indicate standard deviation. ***$P = 0.0001$. (I–K) Egg chambers expressing a control shRNA against *eb1* (H), *dmn* shRNA-A (I), or *dmn* shRNA-B (J) were fixed and processed for immunofluorescence using an antibody against Glued. The shRNAs were expressed using a maternal α-tubulin-Gal4 driver. Bar: A, C, and E = 20 μm; B, D, F, I, J, and K = 50 μm.

factors were all delocalized from the oocyte cortex (Figure 2R; data not shown). In the rest of the oocytes (those containing the large vesicular structures), the endocytic factors remained localized along the cortex (Figure 2, S and S′; data not shown).

Based on these results, we conclude that severe depletion of Dmn results in loss of endocytic factor localization, a compromise in endocytic uptake, and egg chambers that are almost devoid of yolk autofluorescence. Milder depletion of Dmn results in reduced yolk autofluorescence and the accumulation of large vesicles. We hypothesize that the enlarged vesicles represent trapped endocytic intermediates.

Oskar protein and endocytosis

Previous studies have implicated a role for Dynein in the posterior localization of *oskar* messenger RNA (mRNA) (Sanghavi *et al.* 2013). *oskar* mRNA is transcribed by the nurse cells, transported into the oocyte, and localized at the posterior pole (Ephrussi *et al.* 1991; Kim-Ha *et al.* 1991). During transit, *oskar* mRNA is maintained in a translationally repressed state (Kim-Ha *et al.* 1995; Gonsalvez and Long 2012). As such, Oskar protein is only expressed at the posterior of wild-type oocytes. Oskar protein is required for maintaining the anterior–posterior polarity of the oocyte and future embryo (Ephrussi and Lehmann 1992; Smith *et al.* 1992). In addition, Oskar also stimulates endocytosis at the oocyte posterior (Vanzo *et al.* 2007; Tanaka and Nakamura 2008). Given this link between Oskar protein and endocytosis, we examined whether the function of Dmn in endocytosis was dependent on Oskar.

As expected, *oskar* mRNA was localized to the posterior pole in egg chambers expressing a control shRNA (Figure 3A,

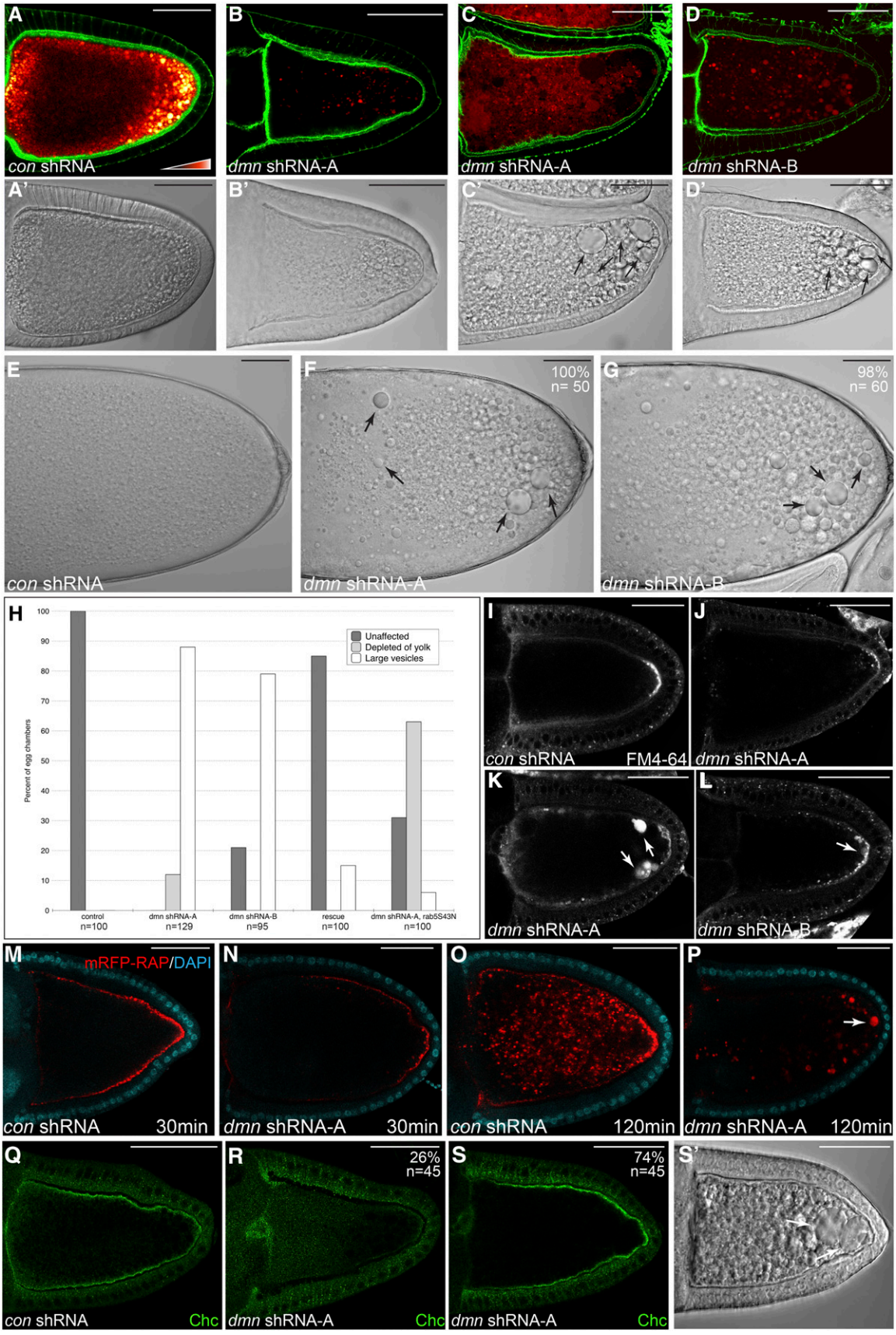

Figure 2 Dmn depletion phenotypes. (A–D) Egg chambers expressing a control shRNA (A), *dmn* shRNA-A (B and C), or *dmn* shRNA-B (D) were fixed and stained to reveal the actin cytoskeleton (green). Autofluorescent yolk particles are displayed using a color-coded range indicator. Black indicates low

arrow). By contrast, *oskar* mRNA was significantly delocalized in egg chambers expressing either *dmn* shRNA-A or *dmn* shRNA-B (Figure 3, B–E). It should be noted that, to visualize delocalized *oskar* mRNA, the Dmn-depleted oocytes had to be imaged at a higher gain setting than the control. In most Dmn-depleted egg chambers, the delocalized signal for *oskar* mRNA was distributed throughout the oocyte with residual enrichment at the posterior pole (Figure 3, B, D, and E, red bars). Occasionally, however, signal for *oskar* mRNA could also be detected within the nurse cell cytoplasm (Figure 3, C and E, arrow, yellow bars). This latter finding is consistent with previous reports indicating a role for Dynein in efficient nurse-cell-to-oocyte transport of *oskar* mRNA (Clark *et al.* 2007; Mische *et al.* 2007).

Two experiments were performed to demonstrate the specificity of the *in situ* hybridization signal. In the first, egg chambers were processed without an RNA probe but were subjected to the tyramide amplification step of the *in situ* hybridization protocol. No signal was observed when these egg chambers were imaged under the same high gain setting as used for Dmn-depleted oocytes (Figure 3F). In a separate experiment, egg chambers were processed using a sense probe against *oskar* mRNA. Despite using five times more sense probe, no signal was detected at the same high gain setting (Figure 3G). Thus, the diffuse signal corresponds to delocalized *oskar* mRNA.

To further validate the *oskar* mRNA phenotype, we examined the localization of Staufen. Staufen is a component of the *oskar* mRNP and is often used as a marker for *oskar* mRNA (Zimyanin *et al.* 2008). Consistent with the *in situ* hybridization result, posterior Staufen localization was severely compromised in Dmn-depleted oocytes (Figure 3, H, I, and J). Based on these results, we conclude that Dmn is required for efficient posterior localization of *oskar* mRNA.

To determine whether Dmn performs a function in endocytosis that is independent of its role in *oskar* mRNA localization, we examined endocytic phenotypes in *oskar* protein-null mutants. Consistent with previous findings (Vanzo *et al.* 2007), *oskar* protein-null mutants displayed reduced yolk autofluorescence (Figure 3, K and L). However, large vesicular structures were not observed in *oskar* protein-nulls (Figure 3L′). In addition, the localization of Chc and Rab5 were relatively unaffected in oocytes lacking Oskar (Figure 3, M and N; data not shown). Occasionally, some regions of the cortex displayed slightly reduced Chc staining (Figure 3N). However, this phenotype was milder in comparison to that observed upon depletion of Dmn (Figure 2R). Thus, reduced yolk autofluorescence is the only endocytic phenotype shared between Dmn-depleted egg chambers and *oskar* protein-null mutants. These results suggest that Dmn has additional roles in endocytosis that are independent from its function in *oskar* mRNA localization.

Specificity of the Dmn depletion phenotype

We next determined whether the Dmn depletion phenotypes could be rescued by transgenic expression of wild-type Dmn. An shRNA-refractory construct was generated in which GFP-Dmn was expressed under the control of the germline-specific *vasa* promoter (GFP-dmn^{ref}) (Sano *et al.* 2002). The shRNA-targeting sequence within this construct was mutated such that it was no longer recognized by the shRNA yet was capable of encoding a wild-type protein (Figure 4A). When this transgene is coexpressed with *dmn* shRNA-A, endogenous Dmn will be depleted. However, mutant phenotypes should be complemented by the transgenic GFP-Dmn^{ref}. For simplicity, we will refer to these as "rescue egg chambers."

GFP-Dmn^{ref} is expressed in the rescue egg chambers and is enriched at the posterior pole (Figure 4B). Furthermore, yolk autofluorescence is restored to wild-type levels in rescue egg chambers (Figure 4C). The vesicular structures that were observed in Dmn-depleted oocytes were seen in only 15% of rescue egg chambers (Figure 2H). The remaining 85% of oocytes resembled wild type (Figure 2H and Figure 4C′). We also examined uptake of mRFP-RAP in control and rescue egg chambers. As noted previously, at 30 min, mRFP-RAP was detected around the entire cortex of control oocytes (Figure 4D). A subtle difference was observed in rescue egg chambers. Although mRFP-RAP was observed at high levels around the cortex, it was often reduced in abundance along the anterior–lateral cortex (Figure 4E). At 120 min of uptake, control oocytes contained abundant mRFP-RAP particles within their interior (Figure 4F). In rescue egg

levels of signal, red indicates moderate signal, and white indicates high levels of signal. DIC images of these egg chambers are shown in A′, B′, C′ and D′. The arrows indicate enlarged vesicular structures. (E–G) DIC images of mature stage 14 egg chambers expressing a control shRNA (E), *dmn* shRNA-A (F), or *dmn* shRNA-B (G) are shown. The penetrance of the indicated phenotypes and the number of egg chambers counted are indicated. (H) Quantification of endocytic phenotypes. Egg chambers from the indicated genotypes were scored for the presence of yolk and large vesicular structures. The percentage of each phenotype observed and the number of egg chambers counted for each genotype are indicated. "Rescue" indicates flies that are coexpressing *dmn* shRNA-A and GFP-dmn^{ref}. *dmn* shRNA-A and *rab5S43N* were coexpressed using the maternal α-tubulin driver. (I–L) Egg chambers expressing a control shRNA (I), *dmn* shRNA-A (J and K), or *dmn* shRNA-B (L) were processed for FM4-64 uptake. The egg chambers were mounted on slides and imaged live. Large vesicles that were positive for FM4-64 are indicated by arrows. (M and N) Egg chambers expressing a control shRNA (M) or *dmn* shRNA-A (N) were processed for mRFP-RAP endocytosis (red). The egg chambers were incubated with mRFP-RAP for 30 min. They were then fixed and stained with DAPI to reveal nuclei (cyan). (O and P) Egg chambers from these same strains were incubated with mRFP-RAP for 120 min to monitor endocytic maturation (red). They were then fixed and stained with DAPI to reveal nuclei (cyan). The arrow indicates enlarged mRFP-RAP endosomes. (Q–S) Egg chambers expressing a control shRNA (Q) or *dmn* shRNA-A (R and S) were fixed and processed for immunofluorescence using an antibody against Chc (green). S′ represents the DIC image of the oocyte in S. The white arrows in S′ indicate enlarged endosomes. The percentage of the phenotypes observed and the number of egg chambers counted are indicated. Bar, 50 μm.

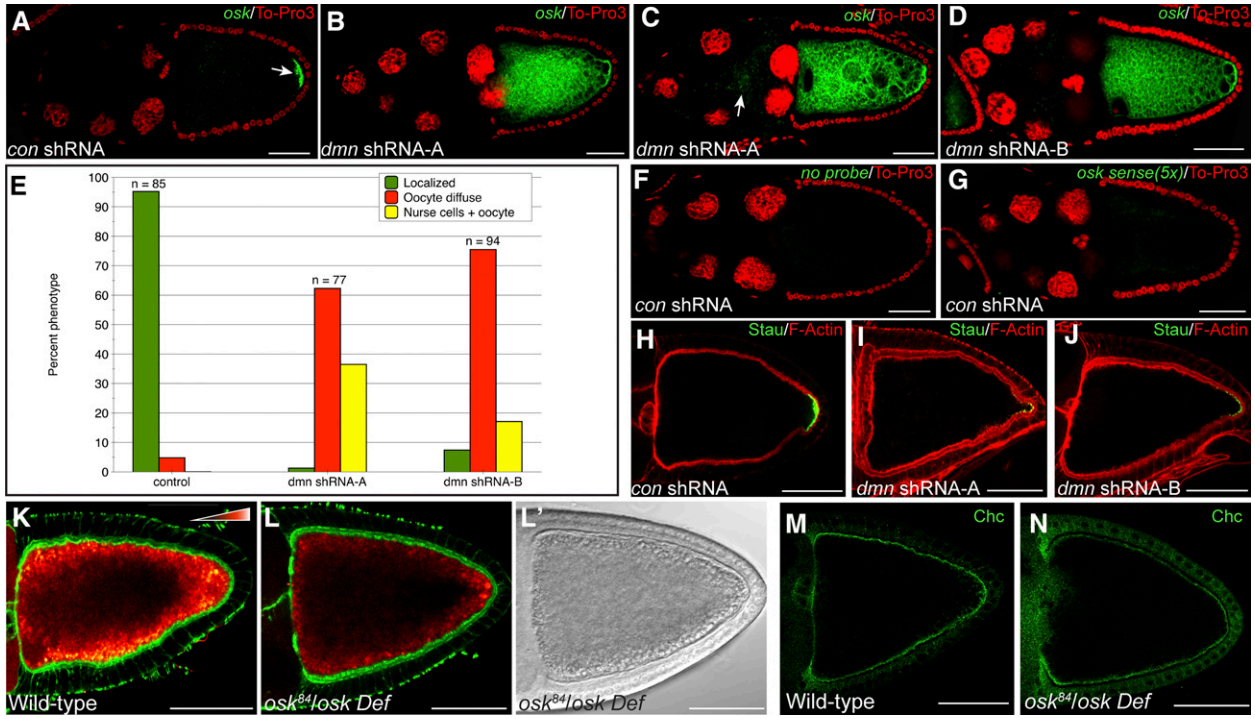

Figure 3 *oskar* mRNA is delocalized in Dmn-depleted egg chambers. (A–D) Egg chambers expressing a control shRNA against *eb1* (A), *dmn* shRNA-A (B and C), or *dmn* shRNA-B (D) were fixed and processed for *in situ* hybridization using an anti-sense probe against *oskar* mRNA (green). The egg chambers were counterstained with ToPro3 to reveal nuclei (red). The egg chambers in B, C, and D were imaged under a higher gain setting in comparison to those in A. This was required to visualize the delocalized *oskar* mRNA signal. (E) Quantification of *oskar* mRNA localization phenotypes. The number of egg chambers counted for each genotype and the percentage of each phenotype observed are indicated. The green bars indicate a wild-type localization pattern. The red bars indicate egg chambers in which signal for *oskar* mRNA is present within the oocyte in a diffuse pattern with residual enrichment at the posterior pole ("Oocyte diffuse"). The yellow bars indicate egg chambers in which *oskar* mRNA signal could be detected within the nurse cell cytoplasm in addition to the oocyte ("Nurse cells + oocyte"). (F) Egg chambers expressing a control shRNA were fixed and processed for *in situ* hybridization. For this experiment, no RNA probe was used, but the egg chambers were processed using the mouse anti-DIG antibody and the tyramide amplification step (green). The egg chambers were imaged under the same gain setting used in B, C, and D. The egg chambers were counterstained with ToPro3 to reveal nuclei (red). (G) Egg chambers expressing a control shRNA were fixed and processed for *in situ* hybridization using a sense probe against *oskar* mRNA (green). Five times more sense probe was used in this experiment in comparison to the anti-sense probe used in A–D. The egg chambers were imaged using the same gain setting as in B, C, and D. The egg chambers were counterstained with ToPro3 to reveal nuclei (red). (H–J) Egg chambers expressing a control shRNA against *eb1* (H), *dmn* shRNA-A (I), or *dmn* shRNA-B (J) were fixed and processed for immunofluorescence using an antibody against Staufen (green). The egg chambers were also counterstained to reveal F-actin (red). (K and L) Egg chambers from wild-type flies (K), or *oskar* protein null flies (L) were fixed and stained to reveal the actin cytoskeleton (green). Autofluorescent yolk particles are displayed using a color-coded range indicator. L′ represents the DIC images of the egg chamber depicted in L. (M and N) Egg chambers from wild-type flies (M) or *oskar* protein null flies (N) were fixed and processed for immunofluorescence using an antibody against Chc (green). Bar, 50 μm.

chambers, mRFP-RAP could be detected within the oocyte interior. However, the particles of mRFP-RAP were slightly enlarged in comparison to the control (Figure 4G). Based on these results, we conclude that GFP-Dmn^{ref} is able to partially rescue the endocytic phenotypes caused by Dmn depletion.

We next examined whether GFP-Dmn^{ref} was able to rescue the *oskar* mRNA localization defect caused by Dmn depletion. As shown in the previous section, *oskar* mRNA was localized to the posterior pole in egg chambers expressing a control shRNA (Figure 4H). A similar pattern was observed in rescue egg chambers (Figure 4I). However, the level of localized *oskar* mRNA was slightly reduced in comparison to the control (Figure 4I). It therefore appears that, although GFP-Dmn^{ref} is able to rescue the *oskar* mRNA localization defect, the level of rescue is not complete.

The reason for not observing complete rescue might have to due with the presence of the GFP tag. The GFP tag might partially affect the function of Dmn. Alternatively, GFP-Dmn^{ref} might not be expressed at sufficiently high levels to completely compensate for loss of endogenous Dmn. Nevertheless, based on the finding that two independent shRNAs produce the same range of phenotypes, and that GFP-Dmn^{ref} is able to partially rescue these phenotypes, it is very likely that the endocytic and *oskar* phenotypes are caused by specific depletion of Dmn.

Blocking endocytic maturation produces enlarged acidic endosomes

To gain insight into the endocytic function of Dmn, we examined phenotypes produced upon disrupting well-characterized components of the endocytic pathway. Dynamin

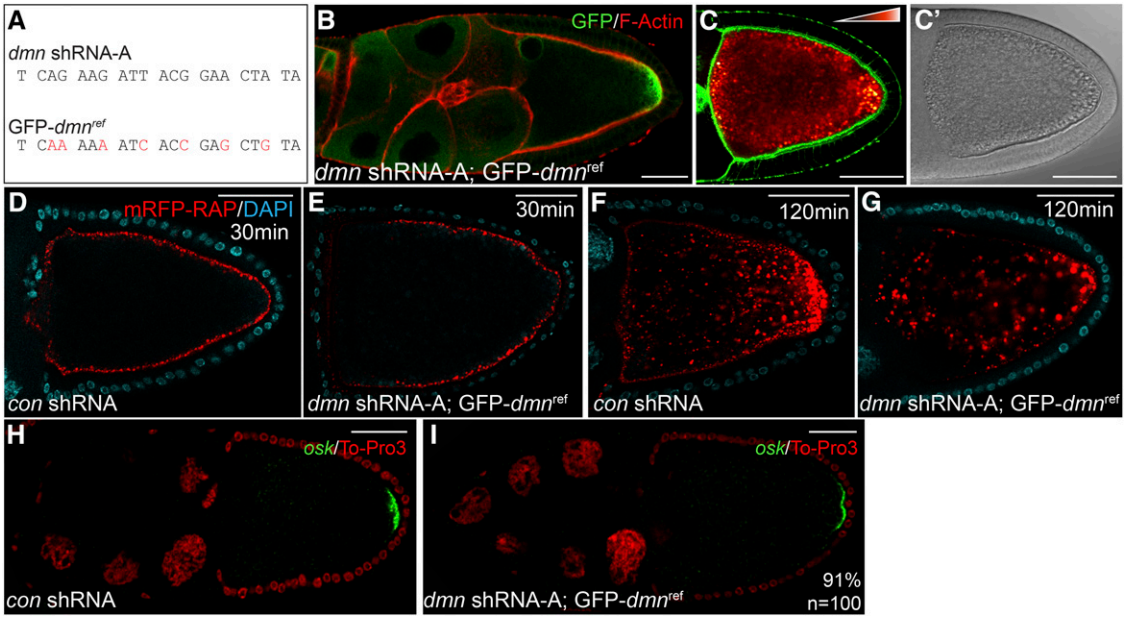

Figure 4 Rescue of Dmn depletion phenotypes. (A) The sequence targeted by *dmn* shRNA-A is indicated. Also indicated are the site-specific mutations made within GFP-*dmn*^{ref} (red). (B) Egg chambers from strains coexpressing *dmn* shRNA-A and GFP-*dmn*^{ref} were fixed and processed for immunofluorescence using an antibody against GFP (green). The egg chambers were also counterstained for F-actin (red). (C) Egg chambers from strains coexpressing *dmn* shRNA-A and GFP-*dmn*^{ref} were fixed and stained to reveal the actin cytoskeleton (green). The autofluorescent yolk particles are displayed using a color-coded range indicator. ADIC image is shown in C′. (D and E) Egg chambers expressing a control shRNA (D) or coexpressing *dmn* shRNA-A and GFP-*dmn*^{ref} (E) were processed for mRFP-RAP endocytosis (red). The egg chambers were incubated with mRFP-RAP for 30 min. They were then fixed and stained with DAPI to reveal nuclei (cyan). (F and G) Egg chambers from these same strains were incubated with mRFP-RAP for 120 min to monitor endocytic maturation (red). They were then fixed and stained with DAPI to reveal nuclei (cyan). (H and I) Egg chambers expressing a control shRNA (H) or coexpressing *dmn* shRNA-A and GFP-*dmn*^{ref} (I) were fixed and processed for *in situ* hybridization using an anti-sense probe against *oskar* mRNA (green). The egg chambers were counterstained with ToPro3 to reveal nuclei (red). Bar, 50 μm.

is a GTPase involved in scission of coated pits at the cell surface (Ramachandran 2011). The *Drosophila* homolog of Dynamin is *shibire* and disrupting its activity results in endocytic defects (Tsuruhara *et al.* 1990; Chen *et al.* 1991; van der Bliek and Meyerowitz 1991). Consistent with these studies, shRNA-mediated depletion of Shibire produced oocytes that were devoid of autofluorescent yolk particles (Supporting Information, Figure S2A). Large vesicles were not observed (Figure S2A′). We next depleted Rab5, a protein that functions at early stages of endocytic maturation, and one that is often used as a marker for early endosomes (Chavrier *et al.* 1990). Consistent with results observed using *rab5* nulls (Compagnon *et al.* 2009), oocytes depleted of Rab5 displayed minimal yolk autofluorescence (Figure S2B). However, large vesicles were not observed in these oocytes (Figure S2B′).

By contrast, disrupting endocytosis at stages downstream of Rab5 produced enlarged endosomes. For example, expression of constitutively active Rab5 prevents maturation of early endosomes to late endosomes. In mammalian cells, this results in enlarged endosomes (Stenmark *et al.* 1994). Expression of Rab5Q88L, a constitutively activated form of *Drosophila* Rab5, produced oocytes with large vesicular structures (Figure 5, A′, B′, and C′). In ~50% of these oocytes, the vesicles emitted a similar level of autofluorescence as the control (Figure 5, A and B). In the remainder, the vesicles emitted elevated levels of autofluorescence (Figure 5C). The example shown in Figure S2C has two adjacent egg chambers. Both of these contain enlarged vesicles (Figure S2C′). However, one of the egg chambers displayed a much higher level of autofluorescence in comparison to the other (Figure S2C). The reason for this heterogeneity is unknown.

Enlarged endosomes were also produced upon shRNA-mediated depletion of Rab7 or upon expression of Rab7T22N, a dominant negative mutant of *Drosophila* Rab7 (Figure 5, D, D′, and E; data not shown). The enlarged vesicles were particularly prominent in stage 14 egg chambers (Figure 5E; data not shown). Rab7 is a component of late endosomes, and in mammalian cells is required for maturation of late endosomes to lysosomes (Huotari and Helenius 2011). It should be noted that the Rab7 disruption phenotype was milder in comparison to phenotypes observed upon depleting Dmn or overexpressing Rab5Q88L. One possible explanation is that the residual Rab7 activity present in these egg chambers ameliorates the endocytic defect. Another possibility is that endocytic maturation can at least partially occur in the absence of Rab7. Consistent with the latter interpretation, enlarged endosomes were more pronounced in mammalian cells depleted of both Rab7 and Rab9 in comparison to cells depleted of just Rab7 (Girard *et al.* 2014).

Collectively, these results suggest that enlarged endosomes are produced when endocytic maturation is blocked downstream

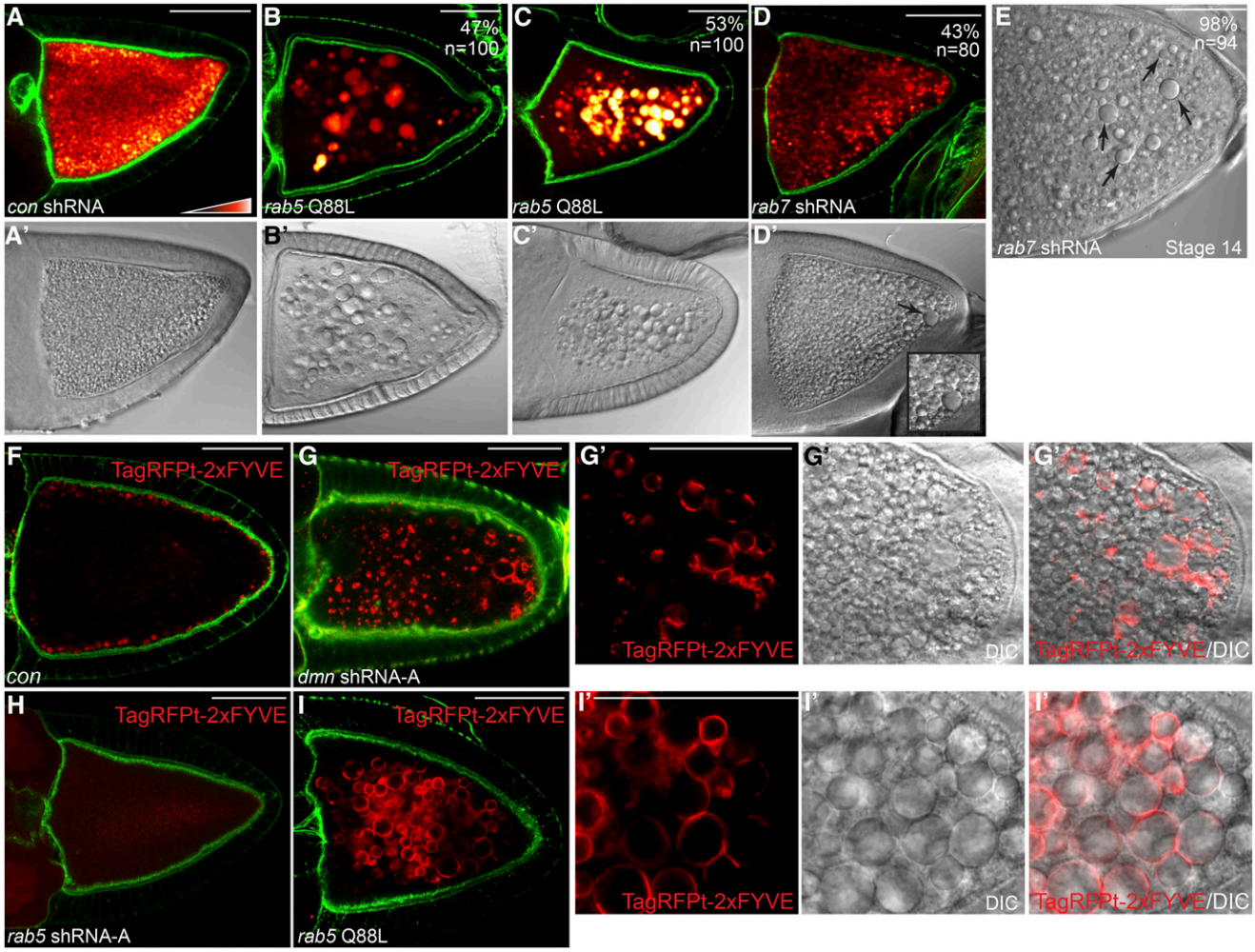

Figure 5 Blocking endocytic maturation produces enlarged endosomes. (A–E) The following strains were fixed and stained to reveal the actin cytoskeleton: *con* shRNA (A), *rab5* Q88L (B and C), and *rab7* shRNA (D and E). The shRNAs and the *rab5* Q88L construct were expressed using the maternal α-tubulin-Gal4 driver. The autofluorescent yolk particles are displayed using a color-coded range indicator. DIC images of these egg chambers are in A′, B′, C′, and D′. A stage 14 egg chamber expressing *rab7* shRNA is shown in E. The efficacy of Rab5 and Rab7 depletion is shown in Figure S1, A–D. (F and G) Egg chambers from a strain expressing TagRFPt-2xFYVE (F) or from a strain coexpressing *dmn* shRNA-A and TagRFPt-2xFYVE (G) were fixed and stained to reveal the actin cytoskeleton (green). The inset in D′ shows enlarged endosomes that are present in the Dmn-depleted strain (G′). (H) Egg chambers from a strain coexpressing *rab5* shRNA and TagRFPt-2xFYVE were fixed and stained to reveal the actin cytoskeleton (green). (I) Egg chambers from a strain coexpressing *rab5* Q88L and TagRFPt-2xFYVE were fixed and stained to reveal the actin cytoskeleton (green). The enlarged RFP-positive vesicles observed upon overexpression of constitutively active Rab5 are indicated (I′). Bar, 50 μm.

of Rab5. To test this hypothesis, we examined the localization of vesicles containing phosphatidylinositol 3-phosphate (PI3P), a lipid modification that occurs downstream of Rab5 (Christoforidis *et al.* 1999). A tool commonly used to visualize PI3P vesicles is the 2xFYVE reporter (Gillooly *et al.* 2000). Recruitment of Vps34 by Rab5 generates PI3P on membranes of early endosomes, enabling their recognition by the 2xFYVE reporter (Christoforidis *et al.* 1999; Behnia and Munro 2005). In control oocytes, RFP-2xFYVE vesicles were localized adjacent to the cortex (Figure 5F). In Dmn-depleted oocytes, the RFP-2xFYVE vesicles were much larger and were distributed throughout the oocyte (Figure 5, G and G′).

The observation that many of the enlarged endosomes in Dmn-depleted oocytes were positive for RFP-2xFYVE indicates that they are formed downstream of Rab5. The 2xFYVE reporter has been extensively used in mammalian cell culture experiments. However, this is the first use of the 2xFYVE reporter in *Drosophila* oocytes. To validate this reporter, we examined whether RFP-2xFYVE vesicles would be present in Rab5-depleted egg chambers. RFP signal was observed in Rab5-depleted oocytes, but was not localized to vesicles (Figure 5H). By contrast, enlarged endosomes produced upon Rab5Q88L overexpression were positive for RFP-2xFYVE (Figure 5, I and I′). Thus, as in mammals, formation of PI3P vesicles in *Drosophila* occurs downstream of Rab5.

We observed a subtle difference in the localization of RFP-2xFYVE in Dmn-depleted oocytes in comparison to Rab5Q88L overexpressing oocytes. In Rab5Q88L oocytes, the RFP-2xFYVE signal was often present uniformly around the entire circumference of enlarged vesicles (Figure 5I). By contrast,

the RFP-2xFYVE signal was present in a more sporadic pattern around the circumference of the enlarged endosomes in Dmn-depleted oocytes (Figure 5G). At present, the mechanistic reason for this difference is unclear.

In many cell types, late endosomes fuse with acidic organelles known as lysosomes. Condensed yolk granules are thought to be modified lysosomes that serve a storage function rather than a degradative role. Whether the condensed yolk granule represents an acidic structure, however, is unknown. We examined stage 10 oocytes using the dye Lysotracker. Lysotracker emits very little fluorescence in a neutral environment, but fluoresces brightly with a drop in pH. Given that the yolk granule is a storage organelle, we were surprised to find that yolk granules in control oocytes were Lysotracker-positive (Figure 6A). In fact, yolk granules emitted much more Lysotracker signal than the traditional lysosomes present in the overlying somatic follicle cells (Figure 6, A and A′). The one population of follicle cells that displayed high levels of Lysotracker signal were the migratory border cells (data not shown). Lysotracker signal is represented in these images using the same black-to-red color-coded range indicator that was used in previous experiments. To ensure that the Lysotracker signal was not in fact autofluorescent yolk, we imaged egg chambers that were not incubated with the dye under the same setting. Under these conditions, no signal was observed (data not shown).

We next examined Dmn-depleted oocytes. The enlarged endosomes in Dmn-depleted oocytes were also Lysotracker-positive (Figure 6, B, B′, C, and C′). By contrast, Rab5-depleted oocytes were almost completely negative for Lysotracker signal (Figure 6, D and D′). Thus, acidification appears to occur downstream of Rab5. Consistent with this notion, the enlarged endosomes observed in egg chambers overexpressing constitutively active Rab5 (Rab5Q88L) were also Lysotracker-positive. Approximately 50% of these oocytes displayed similar levels of Lysotracker signal as control oocytes (Figure 6, E and E′). The remainder displayed very high levels of Lysotracker signal (Figure 6, F and F′). The reason for these pleiotropic phenotypes is unknown. Finally, enlarged endosomes observed upon depletion of Rab7 or upon overexpression of dominant negative Rab7 (Rab7T22N) were also Lysotracker positive (Figure 6, G, G′, H, and H′).

The results presented in Figure 5 and Figure 6 suggest that the enlarged endosomes observed in Dmn-depleted oocytes are produced downstream of Rab5. As a final test of this hypothesis, we examined endocytic phenotypes in flies that were depleted of Dmn and simultaneously overexpressing dominant negative Rab5 (Rab5 S43N). Consistent with our hypothesis, the number of egg chambers containing enlarged endosomes was significantly reduced under these conditions (Figure 2H; Figure S2, D and E).

Ultrastructural analysis of Dmn-depleted oocytes

Control and Dmn-depleted oocytes were next examined using electron microscopy. Condensed yolk granules were abundant in control oocytes (Figure 7A, YG). In contrast, oocytes expressing *dmn* shRNA-A contained significantly fewer yolk granules (Figure 7B). At higher magnification, numerous coated pits and vesicles were detected along the entire oocyte cortex of control egg chambers (Figure 7C, arrows). Although the Dmn-depleted oocyte was not devoid of coated pits and vesicles (Figure 7D, arrows), they were sparsely detected at the oocyte cortex (Figure 7E). The example shown in this EM image most likely corresponds to those egg chambers that exhibit minimal yolk autofluorescence and in which endocytic factors such as Chc are largely delocalized from the cortex. We interpret these egg chambers to be compromised in endocytic uptake.

However, even these Dmn-depleted egg chambers contained numerous endocytic intermediate structures. For example, electron-lucent endosomes containing intraluminal vesicles were observed (Figure 7, D and E, arrowheads). In addition, endosomes containing partially condensed yolk were also seen (Figure 7, D and E, asterisks). Within this category, a qualitative difference was noted between Dmn-depleted and control oocytes. In control oocytes, yolk proteins detach from the membrane of early endosomes and condense into an electron-dense aggregate within the lumen of the vesicle (Figure 7C, asterisks). By contrast, in Dmn-depleted oocytes, yolk proteins remained attached to the membrane of enlarged endosomes in a partially condensed state (Figure 7, D and E, asterisks and arrowheads).

Similar, but milder, phenotypes were observed in egg chambers expressing *dmn* shRNA-B. The number of condensed yolk granules were higher in these oocytes in comparison to those expressing *dmn* shRNA-A (Figure S3, A and B). However, as with the more severely affected strain, oocytes expressing *dmn* shRNA-B contained a large number of endocytic intermediates (Figure 7F; Figure S3, C and D).

Collectively, these findings suggest that Dmn functions directly or indirectly in promoting maturation of early endosomes into mature condensed yolk granules. A defect in these processes results in fewer condensed yolk granules and a concurrent increase in the number of endocytic intermediates.

Microtubule polarity in Dmn-depleted egg chambers

One explanation for the endocytic defects that are observed upon Dmn depletion is that oocyte microtubules are compromised. We therefore examined microtubule organization using several markers. The first maker used was an antibody against α-tubulin. Control oocytes contained a dense arrangement of microtubules at the anterior margin of the oocyte and along the cortex (Figure 8A). The organization of microtubules along the anterior of Dmn-depleted oocytes was relatively unaffected (Figure 8B). However, α-tubulin staining was reduced along the cortex in Dmn-depleted oocytes (Figure 8B, arrows).

We next examined the distribution of microtubule plus-ends using a well-characterized reporter in which the motor domain of Kinesin-1 is fused to β-galactosidase (β-gal) (Clark *et al.* 1994). Using this marker, microtubule plus-ends are observed at the posterior pole of stage 9 and 10a oocytes (Clark *et al.* 1994). This polar distribution is lost by stage

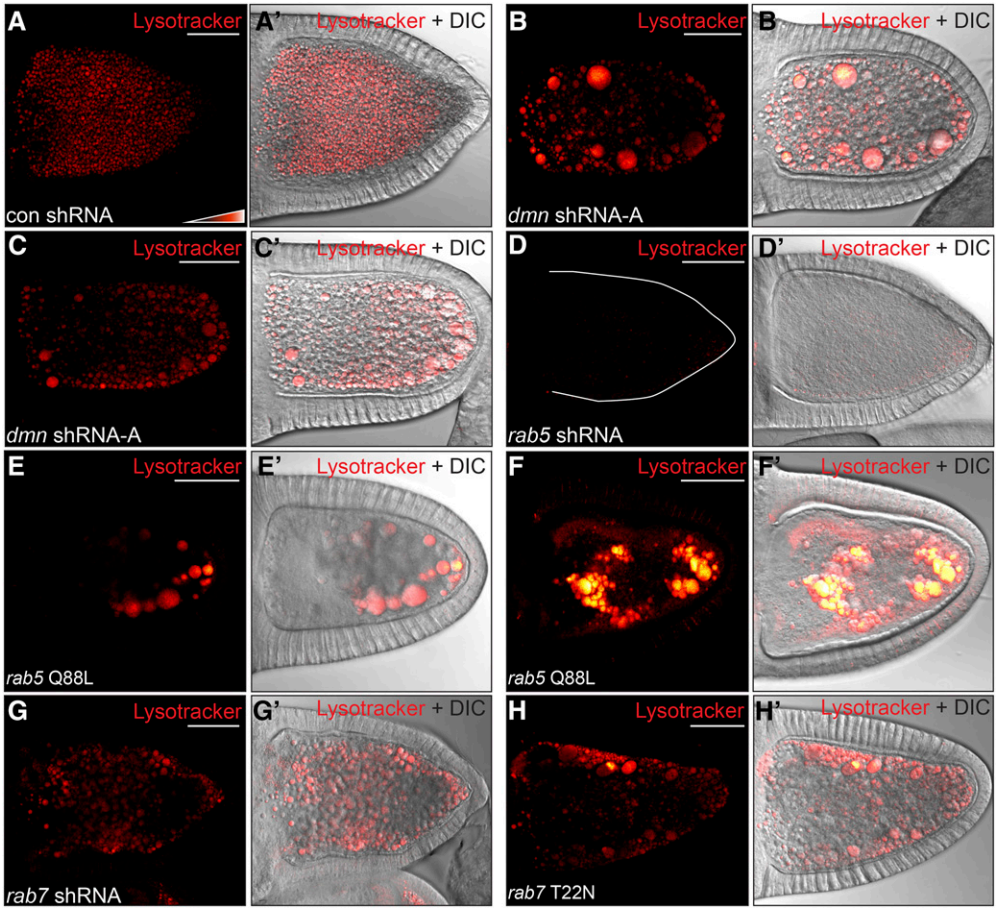

Figure 6 The enlarged vesicles are Lysotracker-positive. (A–D) Egg chambers expressing a control shRNA (A), *dmn* shRNA-A (B and C) or *rab5* shRNA (D) were processed live for Lysotracker staining. The egg chambers were then fixed and imaged. Lysotracker signal is displayed using a color-coded range indicator. Black pixels represent no signal, red pixels represent moderate levels of signal, and white pixels represent high signal. (E and F) Egg chambers expressing *rab5* Q88L using the maternal α-tubulin-Gal4 driver were processed as in A. Approximately 50% of these egg chambers contained enlarged endosomes that displayed a similar level of Lysotracker staining as control oocytes (E and E′). The remainder contained enlarged endosomes that displayed a very high level of Lysotracker staining (F and F′). (G and H) Egg chambers expressing *rab7* shRNA (G) or *rab7* T22N (H) using the maternal α-tubulin-Gal4 driver were processed as in A. Depletion of Rab7 (G and G′) or overexpression of dominant negative Rab7 (H and H′) produced Lysotracker-positive enlarged endosomes.

10b (Clark *et al.* 1994). The localization of Kinesin β-gal was similar in control and Dmn-depleted stage 9 egg chambers (Figure 8, C, D, and E, arrow). By contrast, in stage 10a egg chambers, the posterior localization of Kinesin β-gal was reduced upon Dmn depletion (Figure 8, F, G, and H, arrows).

Oskar protein is involved in recruiting microtubule plus-ends to the oocyte posterior (Zimyanin *et al.* 2007; Sanghavi *et al.* 2012). As noted previously, Dmn depletion results in strong delocalization of *oskar* mRNA (Figure 3). Because translation of *oskar* mRNA is linked to its posterior localization, the level of Oskar protein is reduced upon Dmn depletion (data not shown). As a result of this reduction in Oskar protein, the posterior localization of Kinesin β-gal is compromised in Dmn-depleted egg chambers. However, this is unlikely to be the cause of the observed endocytic phenotypes. As shown previously, *oskar* protein null oocytes do not contain enlarged endocytic vesicles, and the localization of Chc is relatively unaffected (Figure 3, L′ and N). In addition, endocytic intermediates similar to those described in Figure 7 were not seen in *oskar* protein nulls (Vanzo *et al.* 2007). However, Zimyanin *et al.* have shown that posterior Kinesin β-gal localization is severely compromised in *oskar* protein null oocytes (Zimyanin *et al.* 2007). Thus, a reduction in posterior microtubule plus-ends is not associated with the same range of endocytic phenotypes as Dmn depletion.

Finally, we examined the distribution of microtubule minus-ends using an antibody against γ-tubulin. Although the staining of γ-tubulin within follicle cells was somewhat irregular, we observed a consistent reduction in the level of cortically localized γ-tubulin within the oocyte of Dmn-depleted egg chambers (Figure 8, I, J, and K). Thus, upon depletion of Dmn, the abundance of microtubule minus-ends localized to the oocyte cortex is reduced.

Taken together, these results suggest that microtubule organization is altered upon Dmn depletion. It is therefore possible that this altered microtubule organization is at least partially responsible for the endocytic phenotypes observed upon Dmn depletion. It should be noted, however, that not all microtubule-dependent processes were affected. For example, the oocyte nucleus was able to migrate toward the anterior of the oocyte upon Dmn depletion. Anterior migration of the oocyte nucleus requires a polarized microtubule cytoskeleton (Zhao *et al.* 2012). Although anchoring of the oocyte nucleus at the anterior cortex was sometimes compromised in Dmn-depleted oocytes, the initial migration of the nucleus away from the posterior pole was unaffected (data not shown). In fact, enlarged endosomes were often detected in oocytes with a correctly positioned nucleus (Figure S2, F and F′). In addition, despite the fact that *oskar* mRNA was delocalized in Dmn-depleted egg chambers, the mRNA was diffusely distributed and did not accumulate in foci

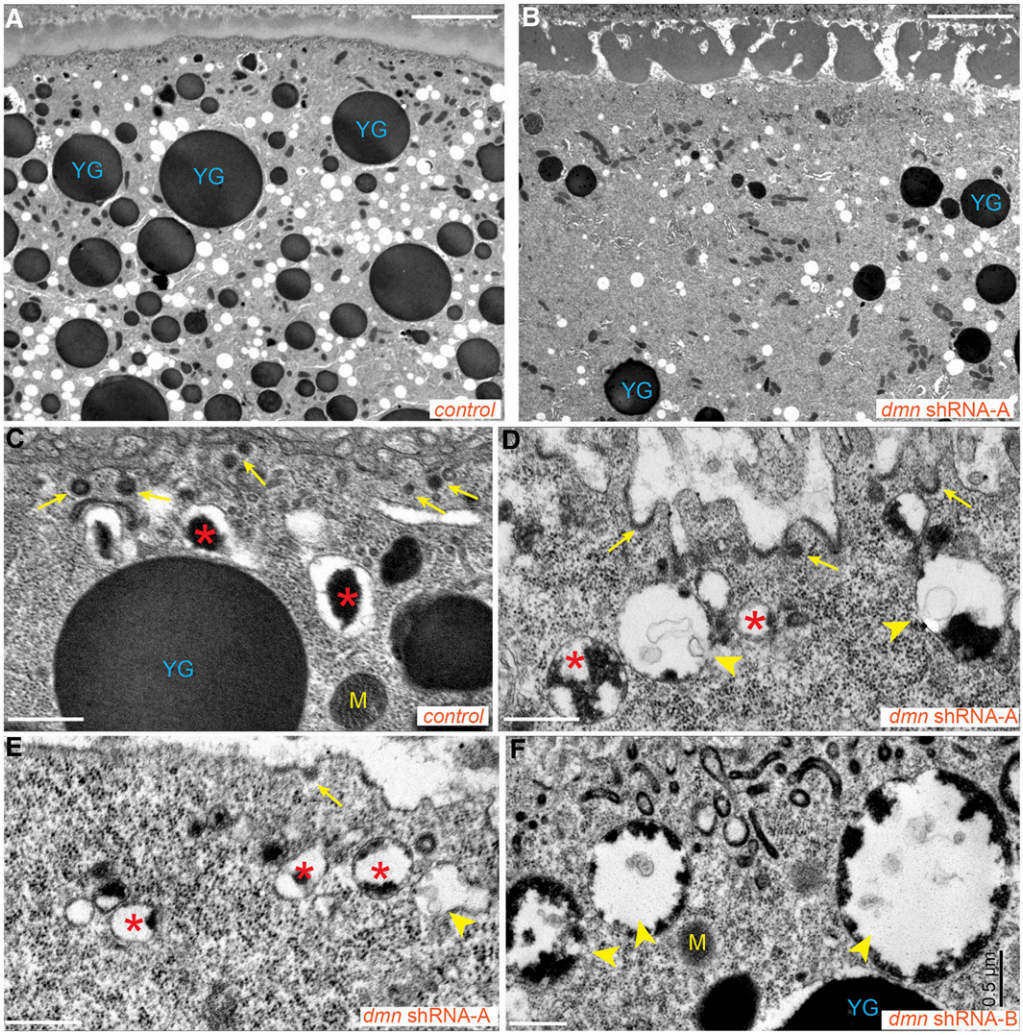

Figure 7 Ultrastructural analysis of Dmn-depleted oocytes. (A and B) Control egg chambers (A) and egg chambers expressing *dmn* shRNA-A (B) were fixed and processed for electron microscopy. Bar, 5 µm. (C–F) High-magnification views of control egg chambers (C) and egg chambers expressing *dmn* shRNA-A (D and E) or *dmn* shRNA-B (F). Bar, 500 nm. "YG" indicates condensed yolk granules. "M" indicates mitochondria. Arrows indicate coated pits and coated vesicles. Arrowheads indicate endocytic intermediate structures containing some yolk and intraluminal vesicles. Asterisks indicate endocytic vesicles with partially condensed yolk proteins. In most of these vesicles, the yolk proteins remained attached to the membrane.

(Figure 3, B–D). Localization of *oskar* mRNA to discrete foci is often observed in mutants with defective microtubule polarity (Yano *et al.* 2004; Tanaka and Nakamura 2008; Morais-de-Sa *et al.* 2014).

Dynein and Lis1 are required for endocytosis

Dmn is a component of the Dynactin complex, a well-characterized regulator of Dynein (Schroer 2004). To directly test the role of Dynein in endocytosis, we depleted Dhc in mid and late stage egg chambers using a published shRNA (Sanghavi *et al.*, 2013). Depletion of Dhc, the motor subunit of the Dynein complex, produced the full range of phenotypes observed upon Dmn depletion (Figure 9, A–C and E). We next examined the consequence of depleting Lis1, another well-known regulator of Dynein. Because antibodies that are capable of detecting endogenous Lis1 are unavailable, we validated the *lis1* shRNA in S2 cells using a GFP-tagged Lis1 construct. The level of GFP-Lis1 was significantly reduced upon expression of *lis1* shRNA, but not a control shRNA (Figure S1I). We then expressed *lis1* shRNA in stage 10 egg chambers. As with Dhc depletion, yolk autofluorescence was reduced in these egg chambers, and enlarged endosomes were detected (Figure 9, D and E).

We also examined uptake of mRFP-RAP in Dhc- and Lis1-depleted oocytes. As noted previously, mRFP-RAP could be detected around the cortex of control oocyte (Figure 9F). By contrast, Dhc-depleted oocytes were severely compromised in mRFP-RAP uptake (Figure 9G). Cortically localized mRFP-RAP could be detected in Lis1-depleted oocytes, but at a lower level in comparison to the control (Figure 9H). In addition, staining Dhc- and Lis1-depleted oocytes with Lysotracker revealed that the enlarged endosomes were acidic (Figure 9, I–K). These results suggest that, in addition to Dmn, Dynein and its regulator Lis1 are required for efficient endocytosis in *Drosophila* oocytes.

Dynein and BicD localize to the oocyte cortex in an endocytosis-dependent manner

Endocytic factors localize along the oocyte cortex with an enrichment at the posterior pole (Tanaka and Nakamura 2008). Consistent with an endocytic role for Dynein, the motor localized at the oocyte cortex, partially colocalizing with Chc, Rab5, and Rab7 (Figure 10, A–F; data not shown). The same localization was also observed for Glued, a component of the Dynactin complex (data not shown). We attempted to

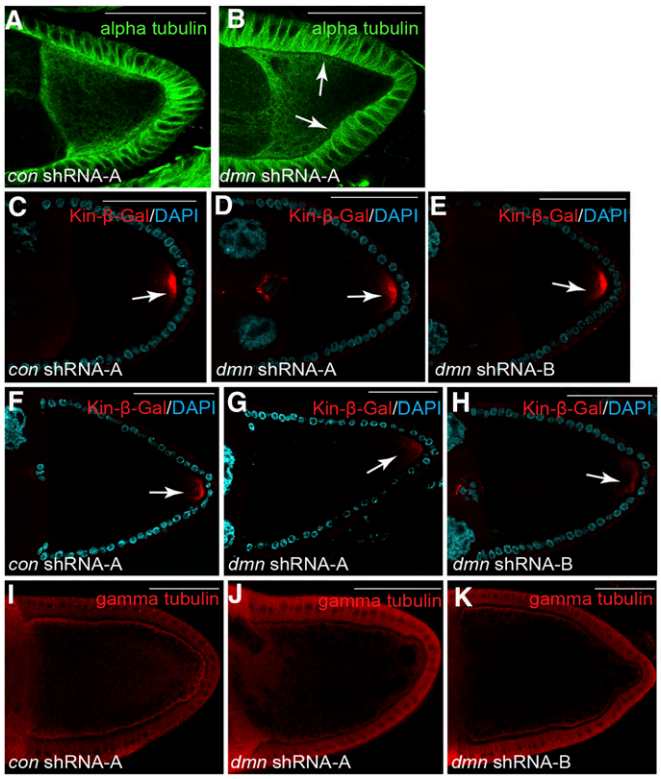

Figure 8 Microtubule polarity in Dmn-depleted oocytes. (A and B) Egg chambers expressing a control shRNA (A) and *dmn* shRNA-A (B) were fixed and processed for immunofluorescence using an antibody against α-tubluin (green). Arrows indicate reduced α-tubulin staining along the cortex of Dmn-depleted egg chambers. (C–E) Egg chambers expressing a control shRNA (C), *dmn* shRNA-A (D), or *dmn* shRNA-B (E) along with the *kinesin β-gal* reporter were fixed and processed for immunofluorescence using an antibody against β-galactosidase (red). The oocytes were also counterstained with DAPI to reveal nuclei (cyan). Kinesin β-gal is a marker for microtubule plus-ends. Stage 9 egg chambers are depicted. The arrow indicates posterior Kinesin β-gal. (F–H) Stage 10 egg chambers from strains expressing a control shRNA (F), *dmn* shRNA-A (G), or *dmn* shRNA-B (H) along with the *kinesin β-gal* reporter were fixed and processed for immunofluorescence using an antibody against β-gal (red). The oocytes were also counterstained with DAPI to reveal nuclei (cyan). The arrow indicates posterior Kinesin β-gal. (I–K) Egg chambers expressing a control shRNA (I), *dmn* shRNA-A (J), or *dmn* shRNA-B (K) were fixed and processed for immunofluorescence using an antibody against γ-tubulin (red). γ-Tubulin is a marker for microtubule minus-ends. Bar, 50 μm.

determine the ultrastructural localization of Dynein and Glued using immunoelectron microscopy. Unfortunately, our efforts using antibodies against these proteins were not successful.

We next determined whether active endocytosis was required for the cortical localization of Dynein. In contrast to control oocytes, Dynein was completely delocalized from the cortex in egg cambers depleted of either Shibire or Rab5 (Figure 10, G and H; data not shown). While this article was in preparation, Vazquez-Pianzola *et al.* demonstrated a role for Bicaudal-D (BicD) in the cortical localization of Chc (Vazquez-Pianzola *et al.* 2014). BicD is an adaptor of the Dynein motor and has been shown to directly interact with Chc (Li *et al.* 2010). We therefore examined the localization of BicD in oocytes that were depleted of Rab5. Although BicD was not excluded from the oocyte cortex, its enrichment at the cortex was lost upon depletion of Rab5 (Figure 10, I and J). By contrast, the localization of Chc was relatively unaffected. Some signal for Chc was detected within the oocyte cytoplasm in Rab5-depleted oocytes (Figure 10, K and L). However, the majority of Chc remained localized along the oocyte cortex (Figure 10, K and L). Based on these results, we conclude that active endocytosis recruits BicD and Dynein to the oocyte cortex.

Discussion

The Dynactin complex has been shown to function as a critical regulator of the minus-end microtubule motor Dynein (Kardon and Vale 2009). A central component of this complex is Dynamitin/p50. Overexpression of Dmn has been shown to dissociate the Dynactin complex, thus resulting in inhibition of Dynein activity (Echeverri *et al.* 1996; Burkhardt *et al.* 1997; Eckley *et al.* 1999; Schroer 2004). More recently, studies have shown that small interfering RNA-mediated depletion of Dmn also results in inhibition of Dynein function (Raaijmakers *et al.* 2013). The goal of this project was to examine the role of Dmn in endocytosis using the *Drosophila* oocyte as a model. Most studies addressing the mechanism of endocytic trafficking use transformed cell lines. The advantage of the *Drosophila* oocyte is that it enables an examination of endocytosis in the context of native tissues.

The primary endocytic cargo of vitellogenic stage egg chambers are the Yolk proteins. Yolk proteins are internalized into the oocyte via clathrin-mediated endocytosis. Subsequent trafficking via the endocytic pathway results in formation of condensed yolk granules (DiMario and Mahowald 1987; Tsuruhara *et al.* 1990; Schonbaum *et al.* 2000). Our findings indicate that Dmn is required for efficient endocytic uptake of Yolk proteins as well as their maturation into condensed yolk granules.

How does Dmn function in endocytosis? The observation that Dhc and Lis1 depletion produces the same range of endocytic phenotypes as Dmn depletion suggests that this function involves regulation of the Dynein motor (Figure 9). In Dmn-depleted oocytes that were severely compromised, Chc was delocalized from the cortex (Figure 2R). Consequently, these oocytes contained only a small number of yolk granules (Figure 2B and Figure 7B). These severely compromised egg chambers reveal a role for Dmn in endocytic uptake. The function of Dynein in endocytic uptake likely involves efficient localization of the Clathrin complex at the oocyte cortex (Figure 10M). This is consistent with recent findings of Vazquez-Pianzola *et al.* who demonstrated a role for the Dynein adaptor BicD in the cortical localization of Chc (Vazquez-Pianzola *et al.* 2014).

Oocytes containing enlarged vesicular structures were also observed upon Dmn depletion. Within this class of more mildly affected egg chambers, Chc remained localized at the oocyte cortex, suggesting that at least some level of endocytic uptake was ongoing (Figure 2S). We interpret this

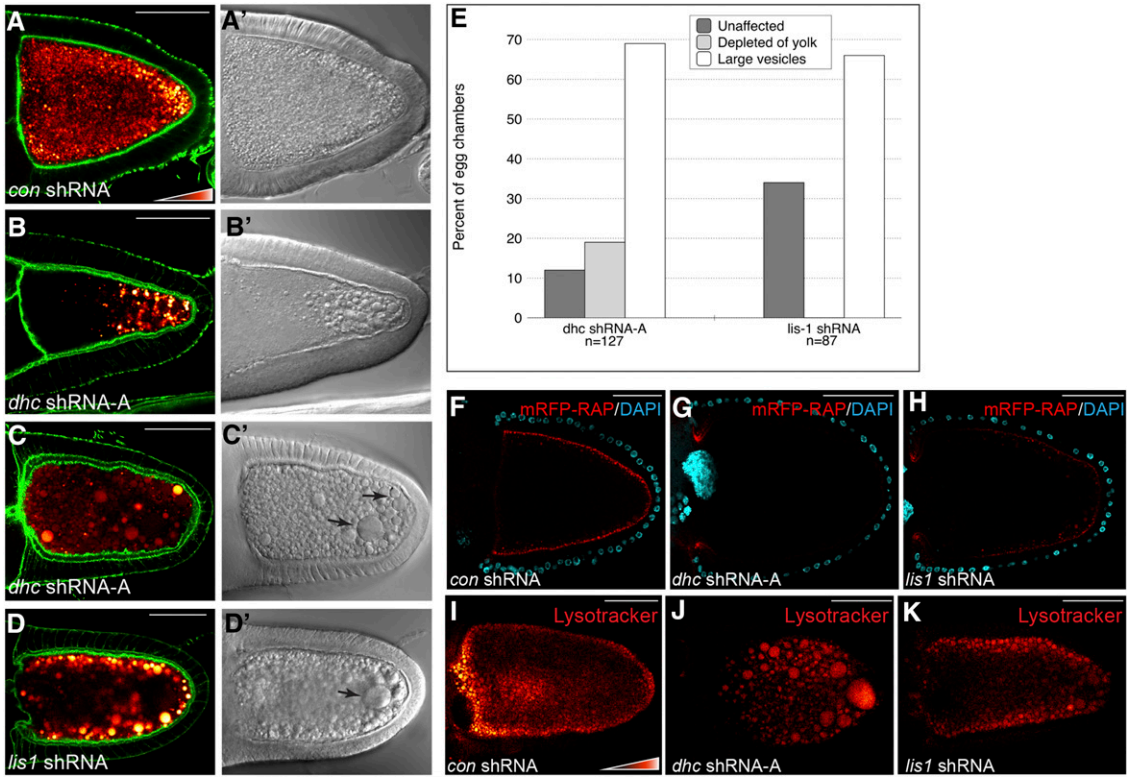

Figure 9 Dynein and Lis1 are required for endocytosis. (A–D) The following strains were fixed and stained to reveal the actin cytoskeleton: *con* shRNA (A), *dhc* shRNA-A (B and C), and *lis1* shRNA (D). The shRNAs were expressed using a maternal α-tubulin-Gal4 driver. Autofluorescent yolk particles are displayed using a color-coded range indicator. DIC images of these egg chambers are shown in A′, B′, C′, and D′. The efficacy of Lis1 depletion is shown in Figure S1I. (E) Quantification of endocytic phenotypes. Egg chambers from the indicated genotypes were scored for the presence of yolk and large vesicular structures. The percentage of each phenotype observed and the number of egg chambers counted for each genotype are indicated. (F–H) Egg chambers expressing a control shRNA (F), *dhc* shRNA-A (G), or *lis1* shRNA (H) were processed for mRFP-RAP endocytosis (red). The egg chambers were incubated with mRFP-RAP for 30 min. They were then fixed and stained with DAPI to reveal nuclei (cyan). (I–K) Egg chambers expressing a control shRNA (I), *dhc* shRNA-A (J), or *lis1* shRNA (K) were processed for Lysotracker staining. The Lysotracker signal is shown using a color-coded range indicator. Bar, 50 μm.

class of oocytes to be compromised in endocytic maturation. We hypothesize that the enlarged vesicles represent stalled endocytic intermediates (Figure 10M and Figure S4).

An alternative explanation for the enlarged structures is that they represent a defect in the biosynthetic pathway and are produced as a consequence of defective exocytosis. Several genes that function in the secretory pathway, such as *jagunal* (*jagn*), *sec5*, and *trailer hitch* (*tral*), have been characterized. In these mutants, the Yl receptor either was absent along the anterior–lateral cortex or was mis-localized within cytoplasmic foci (Murthy and Schwarz 2004; Sommer *et al.* 2005; Wilhelm *et al.* 2005; Lee and Cooley 2007). This was not the case in Dmn-depleted oocytes (Figure S2, G and H). In addition, ultrastructural studies on *jagn* and *sec5* mutant oocytes did not reveal enlarged membrane-bound structures containing intraluminal vesicles (Sommer *et al.* 2005; Lee and Cooley 2007). It is therefore unlikely that these structures are produced due to defects in the biosynthetic pathway. Yet another explanation is that these structures represent aberrant, enlarged lipid droplets. However, the large structures were not labeled with Nile Red, a marker for lipid droplets (Figure S2, I and J) (Yu *et al.* 2011).

As noted above, we favor the hypothesis that these large vesicles represent stalled endocytic intermediates. We further hypothesize that these vesicles are produced at a step that is downstream of Rab5. Several lines of evidence support this interpretation. Expression of constitutively active Rab5 in mammalian cells and *Drosophila* oocytes results in formation of enlarged endosomes (Stenmark *et al.* 1994) (Figure 5, B and C; Figure S4). Depletion of Mon1/Sand-1 in *Caenorhabditis elegans* and *Drosophila* neurons also generates enlarged endosomes (Poteryaev *et al.* 2010; Yousefian *et al.* 2013). Mon1/Sand-1 is involved in conversion of Rab5-positive early endosomes into Rab7-positive late endosomes (Poteryaev *et al.* 2010) (Figure S4). Similarly, depletion of Rab7 in mammalian cells and *Drosophila* oocytes also resulted in formation of enlarged vesicles (Figure 5, D and E) (Vanlandingham and Ceresa 2009; Girard *et al.* 2014). Thus, much like Dmn depletion, blocking endocytic maturation downstream of Rab5 produces enlarged endosomes.

A downstream effector of Rab5 is the kinase Vps34 (Christoforidis *et al.* 1999). Recruitment of Vps34 generates PI3P on membranes of early endosomes (Christoforidis *et al.* 1999; Behnia and Munro 2005) (Figure S4). Many of the

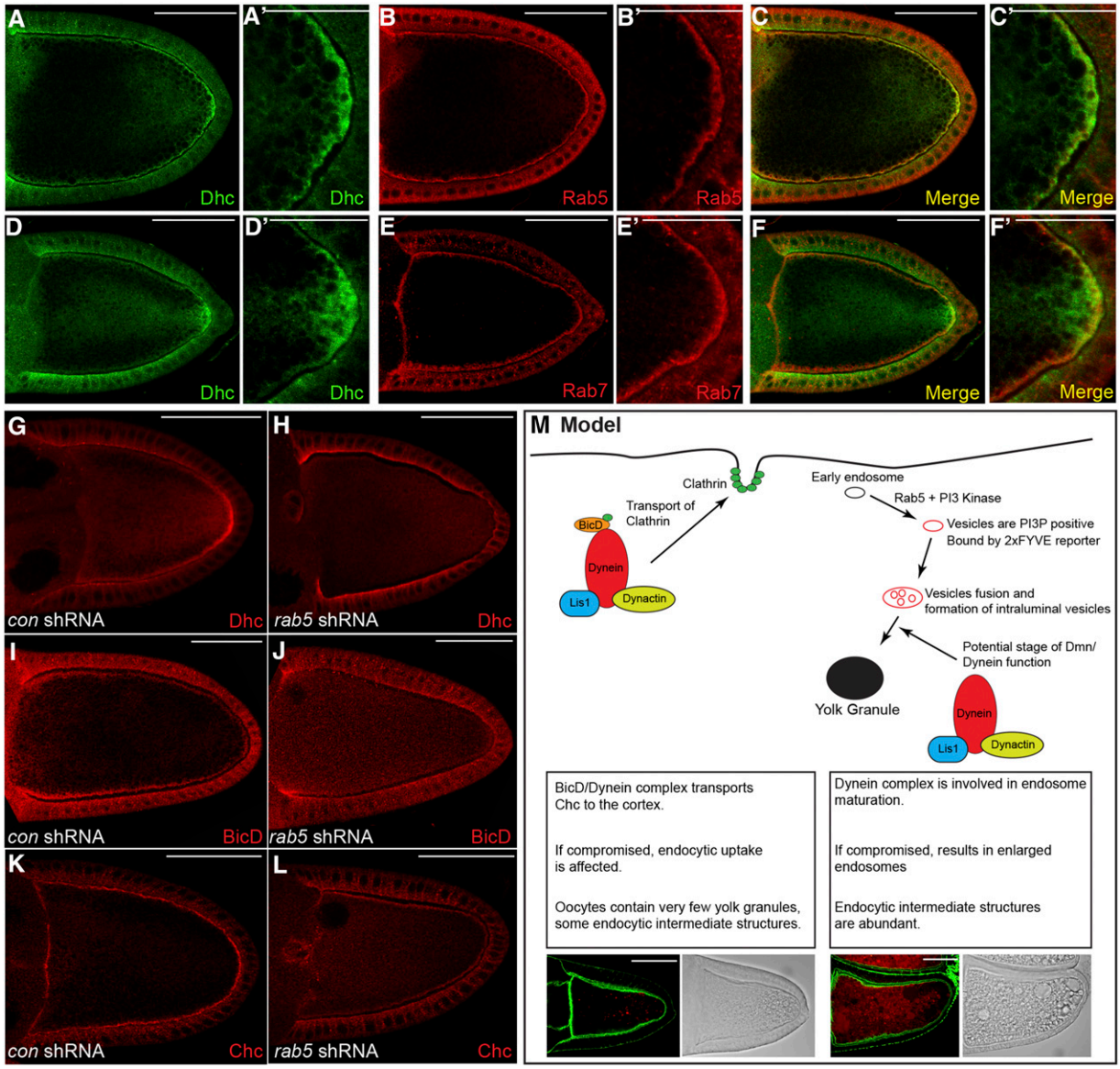

Figure 10 Dynein localizes at the oocyte cortex in an endocytosis-dependent manner. (A–C) Wild-type egg chambers were fixed and processed for immunofluorescence using antibodies against Dhc (A and C, green) and Rab5 (B and C, red). A magnified view is shown in A′, B′, and C′. (D–F) Wild-type egg chambers were fixed and processed for immunofluorescence using antibodies against Dhc (D and F, green) and Rab7 (E and F, red). A magnified view is shown in D′, E′, and F′. (G–L) Egg chambers expressing a control shRNA (G, I, and K) or *rab5* shRNA (H, J, and L) were fixed and processed for immunofluorescence using antibodies against Dhc (G and H), BicD (I and J), or Chc (K and L). Representative oocytes are shown. (M) A model illustrating the role of Dynein in yolk protein endocytosis. We propose that BicD in association with the Dynein motor functions to localize clathrin heavy chain at the oocyte cortex. If this process is compromised, it results in oocytes with minimal yolk granules. In addition, during later stage of endocytosis, we propose that the Dynein complex functions in the maturation of early endosomes into condensed yolk granules. If this process is defective, it results in accumulation of enlarged endocytic intermediates. The intermediates are positive for the 2xFYVE reporter, are acidic, and contain intraluminal vesicles. Bars in A–M: 50 μm; bars in A′, B′, C′, D′, E′, and F′: 25 μm.

enlarged vesicles in Dmn-depleted oocytes were positive for the 2xFYVE reporter, a tool commonly used to detect PI3P membranes (Gillooly *et al.* 2000) (Figure 5G). By contrast, 2xFYVE-positive vesicles were not observed in egg chambers depleted of Rab5 (Figure 5H). In mammalian cells, proteins of the ESCRT complex are known to bind to the PI3P on early endosomes and to induce formation of intraluminal vesicles (Raiborg and Stenmark 2009) (Figure S4). By ultrastructural analysis, we observed numerous endocytic intermediates containing intraluminal vesicles in Dmn-depleted oocytes (Figure 7). These types of vesicles were rarely seen in the control, owing most likely to their rapid conversion to condensed yolk granules (Figure 7) (Schonbaum *et al.* 2000).

Finally, we have demonstrated that the enlarged vesicles in Dmn-depleted oocytes are Lysotracker-positive (Figure 6, B and C). Thus, they represent an acidic compartment. Lysotracker-positive vesicles were absent in egg chambers that were depleted of Rab5 (Figure 6D). However, they were

abundantly detected in egg chambers expressing constitutively active Rab5 or in egg chambers that were depleted of Rab7 (Figure 6, E–H).

Based on these collective observations, we propose that Dmn is required for efficient maturation of early endosomes to late endosomes in the *Drosophila* oocyte (Figure 10M and Figure S4). A slowdown in this process results in formation of enlarged acidic endosomes. These endosomes are PI3P-positive and contain intraluminal vesicles. More than likely, Dmn performs this function in the context of the Dynein motor.

Enlarged endosomes, similar to the kind described in this report, were observed in primary mouse motor neurons that were depleted of BicD1 (Terenzio *et al.* 2014). BicD1 is the mammalian homolog of *Drosophila* BicD. Depletion of BicD1 in motor neurons resulted in delayed sorting of several internalized endocytic cargoes and accumulation of these cargoes within enlarged endosomes (Terenzio *et al.* 2014). Expression of a mutant isoform of the Dynactin component, Glued, in *Drosophila* neurons also resulted in enlarged endosomes that were positive for Rab7 (Lloyd *et al.* 2012). The molecular mechanism leading to the formation of these enlarged endocytic structures remains to be determined.

An important next step is to elucidate the precise role of Dmn and Dynein in endocytic maturation. One potential role for Dmn is in detachment of endocytic cargo from the membrane of early endosomes. In control oocytes, the endocytosed yolk proteins formed electron-dense aggregates within the lumen of maturing endosomes (Figure 7A). By contrast, Dmn depletion produced endocytic intermediates in which the internalized yolk proteins remained attached to the membrane of the vesicle, often failing to coalesce into an electron-dense structure within its center (Figure 7, D, E, and F).

Although numerous factors that function in uptake of yolk proteins into the oocyte have been characterized, very little is known regarding the mechanism by which early endosomes are matured into condensed yolk granules. Ultrastructural studies have been performed on *rab5* null oocytes (Compagnon *et al.* 2009). The mutant oocytes contained clathrin-coated pits and early endosomes but few condensed yolk granules (Compagnon *et al.* 2009). However, large multi-vesicular bodies with yolk proteins still attached to the membrane were not observed (Compagnon *et al.* 2009). Presumably, these structures are formed downstream of Rab5 activity. Further studies will be needed to fully elucidate the mechanism of endocytic maturation in *Drosophila* oocytes.

Acknowledgments

We thank Simon Bullock, Anne Ephrussi, Vladimir Gelfand, Antoine Guichet, and Daniel St. Johnston for providing antibodies and fly strains that were essential for completing this work; Linton Traub for providing the GST-mRFP-RAP construct used in the endocytosis assays; Catherine Rabouille for advice on preparing *Drosophila* egg chambers for electron microscopy; Silvia Corvera for the TagRFP-T-EEA1 plasmid; the Bloomington Stock Center and the Developmental Studies Hybridoma Bank for providing numerous fly strain and antibodies that were critical in completing this work; and Paul McNeil, Anna McNeil, and Tim Kurtz for assistance with various imaging experiments. This work was supported by a grant (1R01GM100088-01) from the National Institutes of Health (to G.B.G.).

Literature Cited

Beguinot, L., R. M. Lyall, M. C. Willingham, and I. Pastan, 1984 Down-regulation of the epidermal growth factor receptor in KB cells is due to receptor internalization and subsequent degradation in lysosomes. Proc. Natl. Acad. Sci. USA 81: 2384–2388.

Behnia, R., and S. Munro, 2005 Organelle identity and the signposts for membrane traffic. Nature 438: 597–604.

Burkhardt, J. K., C. J. Echeverri, T. Nilsson, and R. B. Vallee, 1997 Overexpression of the dynamitin (p50) subunit of the dynactin complex disrupts dynein-dependent maintenance of membrane organelle distribution. J. Cell Biol. 139: 469–484.

Chavrier, P., R. G. Parton, H. P. Hauri, K. Simons, and M. Zerial, 1990 Localization of low molecular weight GTP binding proteins to exocytic and endocytic compartments. Cell 62: 317–329.

Chen, M. S., R. A. Obar, C. C. Schroeder, T. W. Austin, C. A. Poodry *et al.*, 1991 Multiple forms of dynamin are encoded by shibire, a Drosophila gene involved in endocytosis. Nature 351: 583–586.

Christoforidis, S., M. Miaczynska, K. Ashman, M. Wilm, L. Zhao *et al.*, 1999 Phosphatidylinositol-3-OH kinases are Rab5 effectors. Nat. Cell Biol. 1: 249–252.

Clark, A., C. Meignin, and I. Davis, 2007 A Dynein-dependent shortcut rapidly delivers axis determination transcripts into the Drosophila oocyte. Development 134: 1955–1965.

Clark, I., E. Giniger, H. Ruohola-Baker, L. Y. Jan, and Y. N. Jan, 1994 Transient posterior localization of a kinesin fusion protein reflects anteroposterior polarity of the Drosophila oocyte. Curr. Biol. 4: 289–300.

Compagnon, J., L. Gervais, M. S. Roman, S. Chamot-Boeuf, and A. Guichet, 2009 Interplay between Rab5 and PtdIns(4,5)P2 controls early endocytosis in the Drosophila germline. J. Cell Sci. 122: 25–35.

DiMario, P. J., and A. P. Mahowald, 1987 Female sterile (1) yolkless: a recessive female sterile mutation in Drosophila melanogaster with depressed numbers of coated pits and coated vesicles within the developing oocytes. J. Cell Biol. 105: 199–206.

Driskell, O. J., A. Mironov, V. J. Allan, and P. G. Woodman, 2007 Dynein is required for receptor sorting and the morphogenesis of early endosomes. Nat. Cell Biol. 9: 113–120.

Duncan, J. E., and R. Warrior, 2002 The cytoplasmic dynein and kinesin motors have interdependent roles in patterning the Drosophila oocyte. Curr. Biol. 12: 1982–1991.

Echeverri, C. J., B. M. Paschal, K. T. Vaughan, and R. B. Vallee, 1996 Molecular characterization of the 50-kD subunit of dynactin reveals function for the complex in chromosome alignment and spindle organization during mitosis. J. Cell Biol. 132: 617–633.

Eckley, D. M., S. R. Gill, K. A. Melkonian, J. B. Bingham, H. V. Goodson *et al.*, 1999 Analysis of dynactin subcomplexes reveals a novel actin-related protein associated with the arp1 minifilament pointed end. J. Cell Biol. 147: 307–320.

Ephrussi, A., and R. Lehmann, 1992 Induction of germ cell formation by oskar. Nature 358: 387–392.
Ephrussi, A., L. K. Dickinson, and R. Lehmann, 1991 Oskar organizes the germ plasm and directs localization of the posterior determinant nanos. Cell 66: 37–50.
Flores-Rodriguez, N., S. S. Rogers, D. A. Kenwright, T. A. Waigh, P. G. Woodman *et al.*, 2011 Roles of dynein and dynactin in early endosome dynamics revealed using automated tracking and global analysis. PLoS One 6: e24479.
Gillooly, D. J., I. C. Morrow, M. Lindsay, R. Gould, N. J. Bryant *et al.*, 2000 Localization of phosphatidylinositol 3-phosphate in yeast and mammalian cells. EMBO J. 19: 4577–4588.
Girard, E., D. Chmiest, N. Fournier, L. Johannes, J. L. Paul *et al.*, 2014 Rab7 is functionally required for selective cargo sorting at the early endosome. Traffic 15: 309–326.
Gonsalvez, G. B., and R. M. Long, 2012 Spatial regulation of translation through RNA localization. F1000 Biol. Rep. 4: 16.
Hirokawa, N., Y. Noda, Y. Tanaka, and S. Niwa, 2009 Kinesin superfamily motor proteins and intracellular transport. Nat. Rev. Mol. Cell Biol. 10: 682–696.
Huotari, J., and A. Helenius, 2011 Endosome maturation. EMBO J. 30: 3481–3500.
Januschke, J., L. Gervais, S. Dass, J. A. Kaltschmidt, H. Lopez-Schier *et al.*, 2002 Polar transport in the Drosophila oocyte requires Dynein and Kinesin I cooperation. Curr. Biol. 12: 1971–1981.
Jha, A., S. C. Watkins, and L. M. Traub, 2012 The apoptotic engulfment protein Ced-6 participates in clathrin-mediated yolk uptake in Drosophila egg chambers. Mol. Biol. Cell 23: 1742–1764.
Jordens, I., M. Fernandez-Borja, M. Marsman, S. Dusseljee, L. Janssen *et al.*, 2001 The Rab7 effector protein RILP controls lysosomal transport by inducing the recruitment of dynein-dynactin motors. Curr. Biol. 11: 1680–1685.
Kardon, J. R., and R. D. Vale, 2009 Regulators of the cytoplasmic dynein motor. Nat. Rev. Mol. Cell Biol. 10: 854–865.
Kim-Ha, J., J. L. Smith, and P. M. Macdonald, 1991 oskar mRNA is localized to the posterior pole of the Drosophila oocyte. Cell 66: 23–35.
Kim-Ha, J., K. Kerr, and P. M. Macdonald, 1995 Translational regulation of oskar mRNA by bruno, an ovarian RNA-binding protein, is essential. Cell 81: 403–412.
Koch, R., R. Ledermann, O. Urwyler, M. Heller, and B. Suter, 2009 Systematic functional analysis of Bicaudal-D serine phosphorylation and intragenic suppression of a female sterile allele of BicD. PLoS One 4: e4552.
Lee, S., and L. Cooley, 2007 Jagunal is required for reorganizing the endoplasmic reticulum during Drosophila oogenesis. J. Cell Biol. 176: 941–952.
Li, X., H. Kuromi, L. Briggs, D. B. Green, J. J. Rocha *et al.*, 2010 Bicaudal-D binds clathrin heavy chain to promote its transport and augments synaptic vesicle recycling. EMBO J. 29: 992–1006.
Lloyd, T. E., J. Machamer, K. O'Hara, J. H. Kim, S. E. Collins *et al.*, 2012 The p150(Glued) CAP-Gly domain regulates initiation of retrograde transport at synaptic termini. Neuron 74: 344–360.
Mayor, S., J. F. Presley, and F. R. Maxfield, 1993 Sorting of membrane components from endosomes and subsequent recycling to the cell surface occurs by a bulk flow process. J. Cell Biol. 121: 1257–1269.
Mische, S., M. Li, M. Serr, and T. S. Hays, 2007 Direct observation of regulated ribonucleoprotein transport across the nurse cell/oocyte boundary. Mol. Biol. Cell 18: 2254–2263.
Morais-de-Sa, E., A. Mukherjee, N. Lowe, and D. St Johnston, 2014 Slmb antagonises the aPKC/Par-6 complex to control oocyte and epithelial polarity. Development 141: 2984–2992.
Murthy, M., and T. L. Schwarz, 2004 The exocyst component Sec5 is required for membrane traffic and polarity in the Drosophila ovary. Development 131: 377–388.
Navaroli, D. M., K. D. Bellve, C. Standley, L. M. Lifshitz, J. Cardia *et al.*, 2012 Rabenosyn-5 defines the fate of the transferrin receptor following clathrin-mediated endocytosis. Proc. Natl. Acad. Sci. USA 109: E471–E480.
Ni, J. Q., R. Zhou, B. Czech, L. P. Liu, L. Holderbaum *et al.*, 2011 A genome-scale shRNA resource for transgenic RNAi in Drosophila. Nat. Methods 8: 405–407.
Normanno, N., A. De Luca, C. Bianco, L. Strizzi, M. Mancino *et al.*, 2006 Epidermal growth factor receptor (EGFR) signaling in cancer. Gene 366: 2–16.
Poteryaev, D., S. Datta, K. Ackema, M. Zerial, and A. Spang, 2010 Identification of the switch in early-to-late endosome transition. Cell 141: 497–508.
Raaijmakers, J. A., M. E. Tanenbaum, and R. H. Medema, 2013 Systematic dissection of dynein regulators in mitosis. J. Cell Biol. 201: 201–215.
Raiborg, C., and H. Stenmark, 2009 The ESCRT machinery in endosomal sorting of ubiquitylated membrane proteins. Nature 458: 445–452.
Ramachandran, R., 2011 Vesicle scission: dynamin. Semin. Cell Dev. Biol. 22: 10–17.
Rink, J., E. Ghigo, Y. Kalaidzidis, and M. Zerial, 2005 Rab conversion as a mechanism of progression from early to late endosomes. Cell 122: 735–749.
Sanghavi, P., S. Lu, and G. B. Gonsalvez, 2012 A functional link between localized Oskar, dynamic microtubules, and endocytosis. Dev. Biol. **367:** 66–77.
Sanghavi, P., S. Laxani, X. Li, S. L. Bullock, and G. B. Gonsalvez, 2013 Dynein associates with oskar mRNPs and is required for their efficient net plus-end localization in Drosophila oocytes. PLoS One 8: e80605.
Sano, H., A. Nakamura, and S. Kobayashi, 2002 Identification of a transcriptional regulatory region for germline-specific expression of vasa gene in Drosophila melanogaster. Mech. Dev. 112: 129–139.
Schonbaum, C. P., J. J. Perrino, and A. P. Mahowald, 2000 Regulation of the vitellogenin receptor during Drosophila melanogaster oogenesis. Mol. Biol. Cell 11: 511–521.
Schroer, T. A., 2004 Dynactin. Annu. Rev. Cell Dev. Biol. 20: 759–779.
Shaner, N. C., M. Z. Lin, M. R. McKeown, P. A. Steinbach, K. L. Hazelwood *et al.*, 2008 Improving the photostability of bright monomeric orange and red fluorescent proteins. Nat. Methods 5: 545–551.
Skjeldal, F. M., S. Strunze, T. Bergeland, E. Walseng, T. F. Gregers *et al.*, 2012 The fusion of early endosomes induces molecular-motor-driven tubule formation and fission. J. Cell Sci. 125: 1910–1919.
Smith, J. L., J. E. Wilson, and P. M. Macdonald, 1992 Overexpression of oskar directs ectopic activation of nanos and presumptive pole cell formation in Drosophila embryos. Cell 70: 849–859.
Sommer, B., A. Oprins, C. Rabouille, and S. Munro, 2005 The exocyst component Sec5 is present on endocytic vesicles in the oocyte of Drosophila melanogaster. J. Cell Biol. 169: 953–963.
Spradling, A. C., 1994 Developmental genetics of oogenesis, pp. 1–71 in *The Development of Drosophila melanogaster*, edited by M. Bate and A. M. Arias. Cold Spring Harbor Laboratory Press, Cold Spring Harbor, NY.
Stenmark, H., R. G. Parton, O. Steele-Mortimer, A. Lutcke, J. Gruenberg *et al.*, 1994 Inhibition of rab5 GTPase activity stimulates membrane fusion in endocytosis. EMBO J. 13: 1287–1296.
Tan, S. C., J. Scherer, and R. B. Vallee, 2011 Recruitment of dynein to late endosomes and lysosomes through light intermediate chains. Mol. Biol. Cell 22: 467–477.
Tanaka, T., and A. Nakamura, 2008 The endocytic pathway acts downstream of Oskar in Drosophila germ plasm assembly. Development 135: 1107–1117.

Terenzio, M., M. Golding, M. R. Russell, K. B. Wicher, I. Rosewell *et al.*, 2014 Bicaudal-D1 regulates the intracellular sorting and signalling of neurotrophin receptors. EMBO J. 33: 1582–1598.

Tsuruhara, T., J. H. Koenig, and K. Ikeda, 1990 Synchronized endocytosis studied in the oocyte of a temperature-sensitive mutant of Drosophila melanogaster. Cell Tissue Res. 259: 199–207.

Valetti, C., D. M. Wetzel, M. Schrader, M. J. Hasbani, S. R. Gill *et al.*, 1999 Role of dynactin in endocytic traffic: effects of dynamitin overexpression and colocalization with CLIP-170. Mol. Biol. Cell 10: 4107–4120.

van der Bliek, A. M., and E. M. Meyerowitz, 1991 Dynamin-like protein encoded by the Drosophila shibire gene associated with vesicular traffic. Nature 351: 411–414.

Vanlandingham, P. A., and B. P. Ceresa, 2009 Rab7 regulates late endocytic trafficking downstream of multivesicular body biogenesis and cargo sequestration. J. Biol. Chem. 284: 12110–12124.

Vanzo, N., A. Oprins, D. Xanthakis, A. Ephrussi, and C. Rabouille, 2007 Stimulation of endocytosis and actin dynamics by Oskar polarizes the Drosophila oocyte. Dev. Cell 12: 543–555.

Vazquez-Pianzola, P., J. Adam, D. Haldemann, D. Hain, H. Urlaub *et al.*, 2014 Clathrin heavy chain plays multiple roles in polarizing the Drosophila oocyte downstream of Bic-D. Development 141: 1915–1926.

Vonderheit, A., and A. Helenius, 2005 Rab7 associates with early endosomes to mediate sorting and transport of Semliki forest virus to late endosomes. PLoS Biol. 3: e233.

Wilhelm, J. E., M. Buszczak, and S. Sayles, 2005 Efficient protein trafficking requires trailer hitch, a component of a ribonucleoprotein complex localized to the ER in Drosophila. Dev. Cell 9: 675–685.

Yano, T., S. Lopez de Quinto, Y. Matsui, A. Shevchenko, and A. Ephrussi, 2004 Hrp48, a Drosophila hnRNPA/B homolog, binds and regulates translation of oskar mRNA. Dev. Cell 6: 637–648.

Yousefian, J., T. Troost, F. Grawe, T. Sasamura, M. Fortini *et al.*, 2013 Dmon1 controls recruitment of Rab7 to maturing endosomes in Drosophila. J. Cell Sci. 126: 1583–1594.

Yu, Y. V., Z. Li, N. P. Rizzo, J. Einstein, and M. A. Welte, 2011 Targeting the motor regulator Klar to lipid droplets. BMC Cell Biol. 12: 9.

Zhao, T., O. S. Graham, A. Raposo, and D. St. Johnston, 2012 Growing microtubules push the oocyte nucleus to polarize the Drosophila dorsal-ventral axis. Science 336: 999–1003.

Zimyanin, V., N. Lowe, and D. St. Johnston, 2007 An oskar-dependent positive feedback loop maintains the polarity of the Drosophila oocyte. Curr. Biol. 17: 353–359.

Zimyanin, V. L., K. Belaya, J. Pecreaux, M. J. Gilchrist, A. Clark *et al.*, 2008 In vivo imaging of oskar mRNA transport reveals the mechanism of posterior localization. Cell 134: 843–853.

Communicating editor: R. J. Duronio

GENETICS

Supporting Information
www.genetics.org/lookup/suppl/doi:10.1534/genetics.115.180018/-/DC1

Efficient Endocytic Uptake and Maturation in *Drosophila* Oocytes Requires Dynamitin/p50

Guojun Liu, Paulomi Sanghavi, Kathryn E. Bollinger, Libby Perry, Brendan Marshall, Penny Roon, Tsubasa Tanaka, Akira Nakamura, and Graydon B. Gonsalvez

DOI: 10.1534/genetics.115.180018

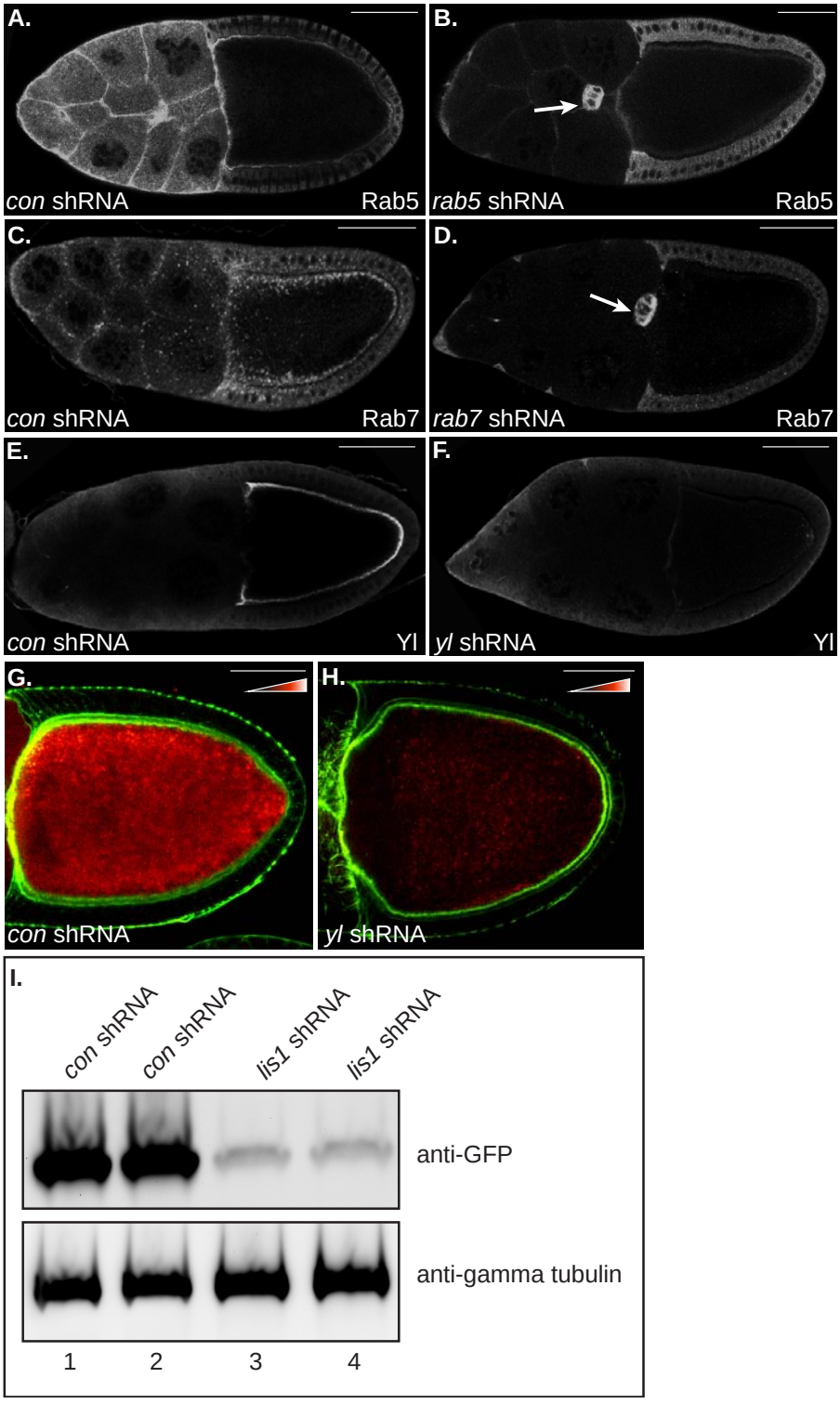

Figure S1 Depletion of Rab5, Rab7, Yl, and Lis1.

A-B. Egg chambers expressing a control shRNA (A) or shRNA against *rab5* (B) were fixed and processed for immunofluorescence using an antibody against Rab5. Representative egg chambers are shown. The arrow indicates somatic border cells. Neither the driver nor the shRNA is expressed in these cells. The border cells therefore represent a good control for the specificity of the depletion.

C-D. Egg chambers expressing a control shRNA (C) or shRNA against *rab7* (D) were fixed and processed for immunofluorescence using an antibody against Rab7. Representative egg chambers are shown. The arrow indicates somatic border cells.

E-F. Egg chambers expressing a control shRNA (E) or shRNA against *yl* (F) were fixed and processed for immunofluorescence using an antibody against Yl. Representative egg chambers are shown.

G-H. Egg chambers expressing a control shRNA (G) or shRNA against *yl* (H) were fixed and stained to reveal the actin cytoskeleton (green). Auto-fluorescent yolk particles are displayed using a color-coded range indicator.

I. Lysates were prepared from *Drosophila* S2 cells co-expressing either a control shRNA against *sh3px1* and GFP-Lis1 (Lanes 1, 2) or *lis1* shRNA-A and GFP-Lis1 (Lanes 3, 4). The lysates were run on an SDS-PAGE gel and examined by western blotting using an antibody against GFP. The blot was subsequently stripped and re-probed using an antibody against gamma-tubulin.

The scale bar on these images represents 50 microns.

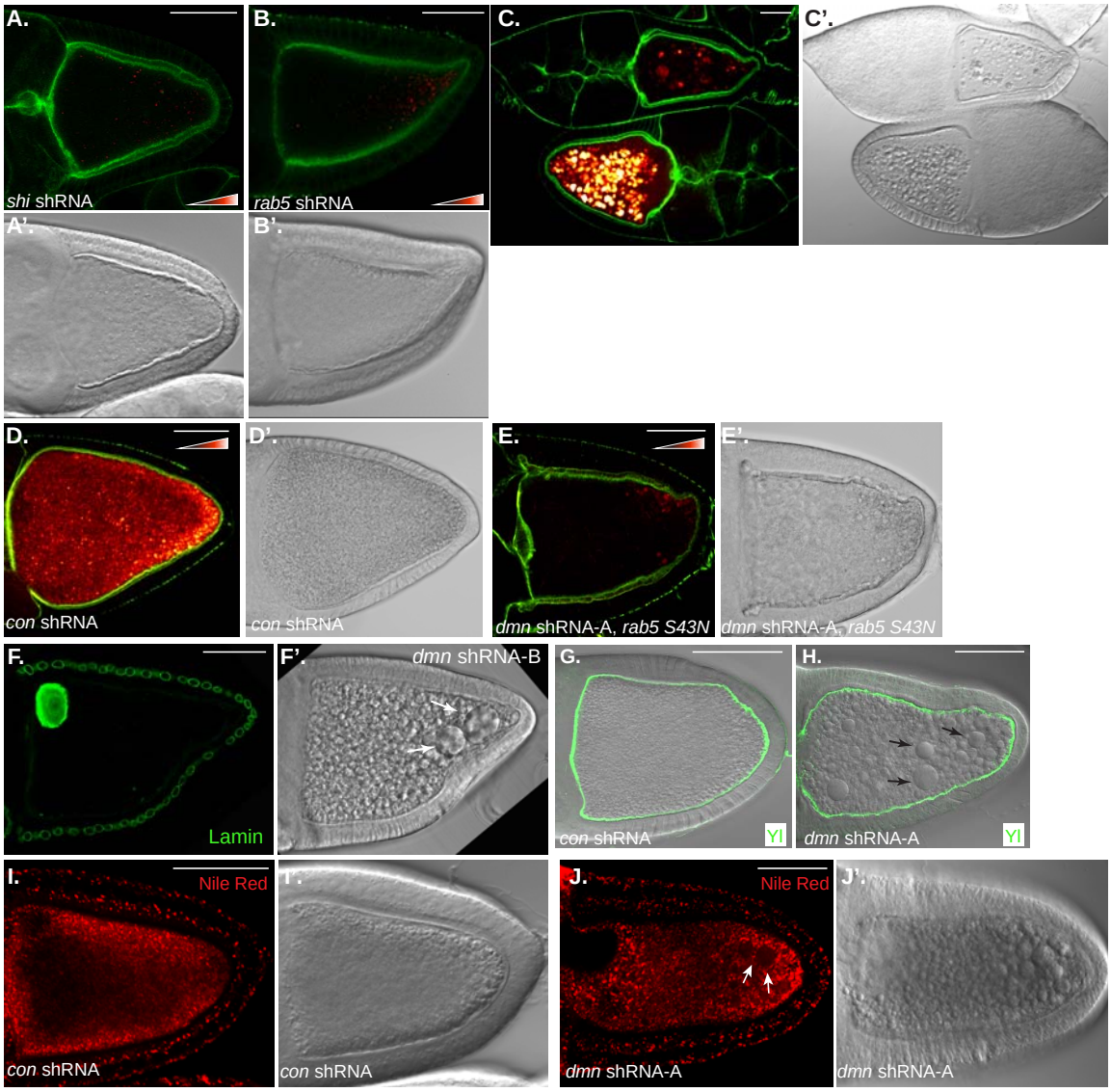

Figure S2 Phenotypes associated with shRNA-mediated depletion.

A-B. Egg chambers expressing an shRNA against *shibire* (A) or *rab5* (B) were fixed and stained to reveal the actin cytoskeleton (green). Auto-fluorescent yolk particles are displayed using a color-coded range indicator. DIC images are shown in A' and B'.

C. Egg chambers from a strain expressing *rab5* Q88L is shown. The egg chambers were fixed and stained to reveal F-actin (green). Yolk auto-fluorescent is displayed using a color-coded range indicator. A DIC image of these egg chambers is shown in C'.

D-E. Egg chamber expressing a control shRNA (D) or co-expressing *dmn* shRNA-A and *rab5S43N* (E) were fixed and stained to reveal the actin cytoskeleton (green). Auto-fluorescent yolk particles are displayed using a color-coded range indicator. DIC images are shown in D' and E'.

F. Egg chambers expressing *dmn shRNA-B* (F) were fixed and stained using an antibody against Lamin DmO (green). The DIC images is shown in F'.

G-H. Egg chambers expressing a control shRNA (G), or *dmn* shRNA-A (H) were fixed and processed for immunofluorescence using an antibody against Yl (green). The immunofluorescence signal was superimposed on the DIC image of the same egg chamber. Arrows indicate enlarged endosomes present in the Dmn depleted oocytes.

I-J. Egg chambers expressing a control shRNA (I) or *dmn* shRNA-A (J) were dissected and processed for Nile Red staining (red). DIC images are shown in I' and J'. The arrows indicate enlarged vesicles that are negative for Nile Red staining.

The scale bar on these images represents 50 microns.

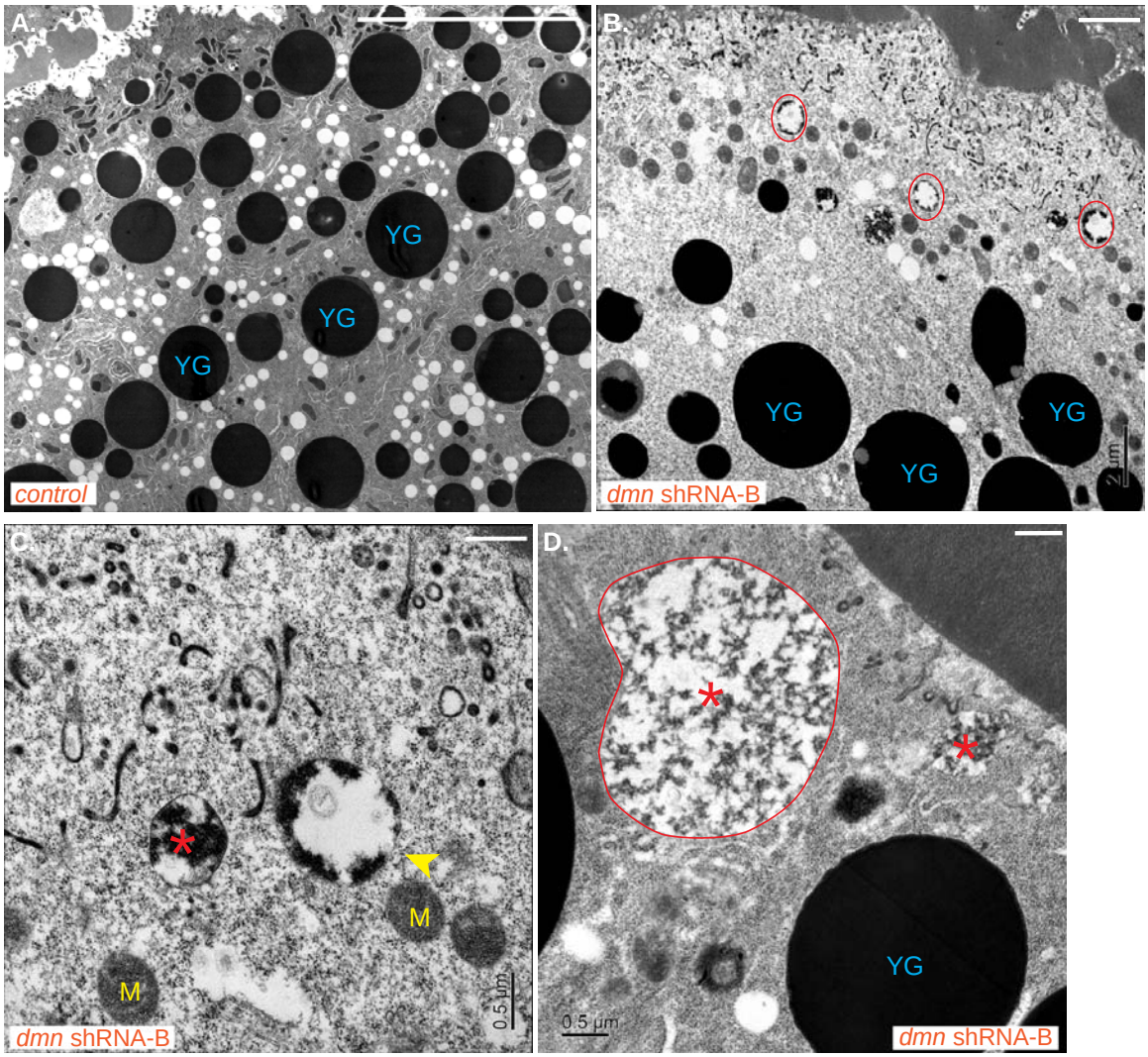

Figure S3 Ultra-structural images of Dmn depleted oocytes.
A. The ultra-structure of an oocyte expressing a control shRNA is shown. The scale bar is 2 microns.

B. The ultra-structure of an oocyte expressing a *dmn* shRNA-B is shown. The scale bar is 2 microns.

C-D. The ultra-structure of oocytes expressing a *dmn* shRNA-B is shown. The scale bar is 0.5 microns.

YG indicates condensed yolk granules. M indicates mitochondria. The red circles indicate endocytic intermediates. The arrowhead indicates endocytic intermediate structures containing some yolk and intraluminal vesicles. The asterisk indicates endocytic vesicles with partially condensed yolk proteins.

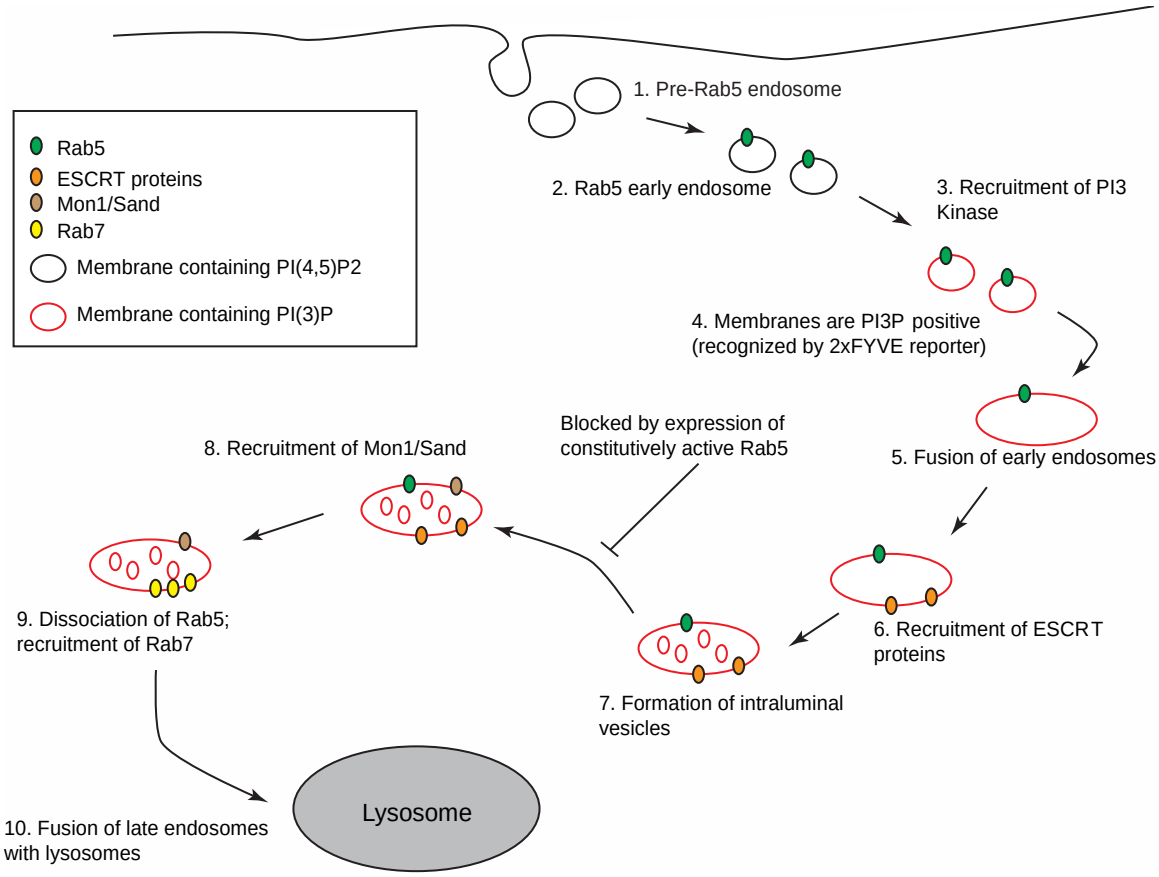

Figure S4 A model of endocytic maturation in mammalian cells.
Upon entry into the cell, some cargoes first traffic through a pre-Rab5 compartment. Subsequently, Rab5 associates with these vesicles. Often, these are referred to as 'early endosomes'. Next, the kinase Vps34 is recruited to these endosomes by Rab5, thus generating phosphatidylinositol 3-phosphate (PI3P) on the membrane of these vesicles. This phosphoinositide modification is recognized by the 2xFYVE reporter. These vesicles also have a tendency to fuse and become larger. Next, proteins of the ESCRT complex are recruited to early endosomes by binding PI3P present on the membrane of these vesicles. The ESCRT complex proteins are responsible for formation of intraluminal vesicles. Subsequently, the protein Mon1/Sand is recruited to these endosomes. The activity of Mon1/Sand results in displacement of Rab5 and in concomitant recruitment of Rab7. These Rab7-positive vesicles are often referred to as 'late endosomes'. Finally, Rab7 promotes the fusion of late endosomes with lysosomes.